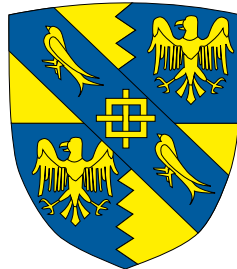


# Particle tracking using light-sheet microscopy



**Craig T. Russell**

Department of Chemical Engineering and Biotechnology  
University of Cambridge

This dissertation is submitted for the degree of  
*Doctor of Philosophy*

Magdalene College

August 2017



I would like to dedicate this thesis to booze



## **Declaration**

I hereby declare that except where specific reference is made to the work of others, the contents of this dissertation are original and have not been submitted in whole or in part for consideration for any other degree or qualification in this, or any other university. This dissertation is my own work and contains nothing which is the outcome of work done in collaboration with others, except as specified in the text and Acknowledgements. This dissertation contains fewer than 65,000 words including appendices, bibliography, footnotes, tables and equations and has fewer than 150 figures.

Craig T. Russell  
August 2017



## **Acknowledgements**

And I would like to acknowledge ...



## **Abstract**

This is where you write your abstract ...



# Table of contents

<b>List of figures</b>	<b>xiii</b>
<b>List of tables</b>	<b>xv</b>
<b>1 Introduction</b>	<b>1</b>
1.1 Scientific Background . . . . .	1
1.1.1 Motivation . . . . .	2
1.1.2 Structure . . . . .	3
1.2 Optical Microscopic Imaging . . . . .	3
1.2.1 Fluorescence . . . . .	4
1.2.2 Widefield Fluorescent Microscopy . . . . .	6
1.3 Three Dimensional Imaging in Life Sciences . . . . .	8
1.3.1 Confocal Microscopy . . . . .	9
1.3.2 Selective Plane Illumination Microscopy Principles . . . . .	10
1.4 Particle Tracking In Life Science . . . . .	15
1.4.1 Particle Spatial Localisation . . . . .	15
1.4.2 Particle Temporal Localisation . . . . .	16
1.4.3 Single Particle Tracking . . . . .	16
1.5 Technologically limited Biological Questions . . . . .	19
1.5.1 Neuro-degenerative Disease . . . . .	19
1.5.2 Virus Trafficking . . . . .	20
<b>2 Contemporary light-sheet technology</b>	<b>21</b>
2.1 Generating Light Sheets . . . . .	22
2.1.1 Light sheet generation . . . . .	22
2.1.2 Optical Light sheet Generation . . . . .	22
2.1.3 Digital Light sheet Generation . . . . .	23

2.1.4	Volumetric imaging . . . . .	23
2.2	Objective Arrangements . . . . .	24
2.2.1	Single View . . . . .	24
2.2.2	Multi-View . . . . .	27
2.3	Single Objective Light Sheet Microscopy . . . . .	28
2.4	Illumination . . . . .	29
2.4.1	Gaussian Techniques . . . . .	29
2.4.2	Exotic Beams . . . . .	30
2.4.3	Thinner Beams . . . . .	31
<b>3</b>	<b>Homographically generated light-sheets</b>	<b>33</b>
3.0.1	Affine region of interest . . . . .	33
3.0.2	Projective region of interest . . . . .	34
3.0.3	Homography and homogenous coordinates . . . . .	35
3.1	Experimental Implementation and Verification . . . . .	37
3.1.1	iSPIM Design . . . . .	37
3.1.2	Scan lens characterisation . . . . .	38
3.1.3	<i>in situ</i> characterisation . . . . .	38
3.2	Conclusions . . . . .	40
<b>4</b>	<b>Light-sheet microscopy combined with remote force measurements</b>	<b>43</b>
4.1	Tissue dynamics in developing organisms . . . . .	45
4.1.1	Embryonic rheology . . . . .	45
4.2	Methods of measuring tissue dynamics . . . . .	45
4.3	Magnetic tweezers combined with Light-sheet microscopy . . . . .	45
4.3.1	Design . . . . .	45
4.4	Results . . . . .	45
4.5	Discussion . . . . .	45
<b>References</b>		<b>47</b>
<b>Appendix A</b>	<b>How to install L<sup>A</sup>T<sub>E</sub>X</b>	<b>51</b>
<b>Appendix B</b>	<b>Installing the CUED class file</b>	<b>55</b>

# List of figures

1.1	Standard jablonski diagram . . . . .	5
1.2	Fluorescent filter cube . . . . .	7
1.3	Rayleigh Limit . . . . .	8
1.4	Airy Disc . . . . .	9
1.5	Confocal microscope principle . . . . .	11
1.6	Confocal resolution improvement . . . . .	11
1.7	Single Plane Imaging Microscope principle . . . . .	12
1.8	Routine to track particles three dimensionally in SPIM . . . . .	18
2.1	(a): The simple SPIM field of view – only a quarter of a sample has optimum illumination (green) and excitation (red). (b): by rotating a sample field of view can be quadrupled but at a cost in acquisition time. (c): By adding extra excitation and detection path the entire sample can be imaged without a rotation. (d): by making optical paths of a LSFM dual purpose a quadrant of a sample can be imaged from two orthogonal perspective and with correct image fusion achieve isotropic resolution. tod . . . . .	26
2.2	. . . . .	27

3.1 (a) Schematic of the light-sheet optics using a large NA detection objective, the beam is scanned in $x$ to create a virtual sheet. (b-e) For best image quality, the illumination planes (shown as red when not perfectly registered to the illumination planes) must be registered to the detections planes (green). The linear registration (c) Tends to produce non-uniform out of focus illumination across the image. The affine registration (d) is commonly used to match the image centres between the top and bottom planes however the projective registration (e) for four control points provides superior performance due to decreased out-of-focus fluorescence. . . . .	34
3.2 <b>Scan lens characterisation</b>   Figure (a) shows the Illumination profile in the $xz$ plane for 400 scan positions, with a 3 pt registration. The beam positions in (a) were each localised by fitting a 2D Gaussian. The identified positions using a 3 pt (c) and 4 pt (b) show that the positional discrepancy of the 3 pt method is largely fixed by the 4 pt registration. . . . .	39
3.3 <b><i>in situ</i> characterisation</b>   (a-b) Ratios of intensity maxima of localised fluorescent bead images were compared in 3D observation volumes using 3 and 4 pt corrections. (a) These ratios show an average 42% increase in contrast for the 4 pt. case, with an increasing effect when traveling axially (b). (c) The corresponding graph for a beam scanned through dye solution also demonstrates greater light capture efficiency which becomes more significant with depth. The image maxima was taken as a good measure of beam to image plane focus. In (d) we show a transgenic Zebrafish expressing mCherry:beta-actinCAAX, in which the membrane contrast is substantially improved by the 4 pt registration. . . . .	40

# **List of tables**



# **Chapter 1**

## **Introduction**

### **1.1 Scientific Background**

This project aims to develop a light sheet microscope imaging system to permit the three dimensional tracking of particles through biological samples. This will be used to monitor how toxic proteins travel between cells and how virus particles infect their host organisms with minimal photo-damage to the sample, using animal models such as drosophila. This system will be based on the work of Ernst Stelzer who pioneered digital light sheet technology [? ].

A light sheet microscope uses orthogonal illumination and detection to optically section biological samples. A previous system was built in order to study developmental biology. This project aims to improve upon this design so as to facilitate a novel particle tracking technique.

The new system will:

- Be more vibrationally stable for low noise tracking
- Accommodate a three dimensional stage for particle tracking and volume imaging with nanometre resolution
- Use structured illumination modes that can provide higher resolution than standard illumination
- Provide more excitation wavelengths to enable improved biological flexibility in terms of fluorescent dyes that can be used with better specificity

- Feature a user-friendly software interface so that users can produce images independently with a strong programming architecture for future collaborative development.

### 1.1.1 Motivation

Viruses are carriers of infectious disease in humans, by hijacking the internal working of the cell the virus replicates using the machinery of the cell. 80 % of adults in the UK are thought to be infected with Herpes Simplex Virus 1 (cold sores) which is currently medically incurable [? ]; only the symptoms can be suppressed. Understanding virus pathology is a requirement for assisting in therapeutic intervention. The virus structure is well understood through high resolution techniques such as Atomic Force Microscopy and Electron Microscopy. In this group we have used super resolution techniques to study the Herpes Simplex Virus 1 structure *in vitro* [? ]. Contemporary biological models of viral infectivity dynamics are based on *in vitro* studies Studying these dynamics *in vivo* and following a virus through its entire process in a living organism could provide new, useful insights and understanding which could be used to suppress or reverse viral infection in humans. Virus particles are smaller than the diffraction limit (20 nm - 200 nm); optical super resolution techniques can image sub-diffraction limit and have observed Human Immunodeficiency Virus 1 [? ]. Virus particles move tens of nanometres on the time scale of milliseconds [? ], these techniques currently do not produce the temporal resolution required to accurately track virus particles [? ] in three dimensions and are limited to *in vitro* studies.

Dementia among the rapidly ageing first world population is becoming a heavy burden on healthcare; as of 2015 there are 850 000 people in the UK suffering with dementia[? ]. Alzheimer's disease (AD) is a neurodegenerative affliction accounting for 62% of all dementia sufferers. Amyloid fibril plaques and neurofibrillary tangles (NTF) are commonly found in post mortem AD sufferers' brains. It is believed that misfolded Amyloid plaques trigger the accumulation of neurofibrillary tangles and a toxic species of microtubule-associated protein, tau [? ? ]. Within our group we have studied Amyloid fibril aggregation using super resolution techniques and the role of tau proteins in neuronal dysfunction. We have demonstrated that extracellular tau can initiate tau pathology in AD [? ], a complimentary *in vivo* study on tau protein's [? ] dynamic propagation in axons would serve to elucidate AD pathology.

These issues can be addressed using light sheet technology. Light sheet microscopes use orthogonal plane illumination to optically section biological samples, allowing an *in vivo* three dimensional study. Confocal microscopy also produces optical sectioning, however its raster scanning nature means it is a slow technique. Orthogonal illumination and detection allows detection rates comparable to wide-field. Light sheet technology is also a low photo-toxicity method compared to confocal and as such can image for extended periods of time at millisecond resolution.

Particle localisation techniques are compatible with light sheet microscopy and can be used to accurately localise particles to sub-pixel, sub-diffraction limited positions in two dimensions. In conjunction with a novel third dimensional tracking technique, exclusive to light sheet, full sub-diffraction limited tracking is viable [? ]. This will then enable the *in vivo* study of virus trafficking through a host cell and protein propagation in neurons with unparalleled temporal resolution.

### 1.1.2 Structure

Here, a light sheet microscope is developed to track particles in three dimensions with millisecond temporal resolution. Firstly the theory of fluorescence microscopy and light sheet microscopy is discussed with a comparison to other similar techniques followed by a review of particle tracking methods which are considered in the context of a light sheet microscope. The current biological model of virus pathology and tau protein propagation and their challenges is then presented. This report then discusses the methods and materials used to build a light sheet microscope up until its current state. Finally the progress of the microscope is summarised and the future work for the project is discussed in terms of experiments needed (once the system is operational) to determine its ability and limitations when applied to virus and tau protein tracking.

## 1.2 Optical Microscopic Imaging

Biological processes occur at the sub micrometer-nanometre scale and thus can be studied using optical microscopes [? ]. The essential components of an optical microscope have not changed in over 200 years [? ? ]. These components are: a condenser lens, to concentrate illumination into the sample; an objective lens, to collect and magnify the emissions from the sample and a tube lens to focus the light

from the objective onto the image plane and an eyepiece, now more commonly a digital camera for recording. With the discovery of fluorescence and development of fluorescent proteins (labels), contrast and sensitivity improved dramatically. This section will briefly introduce the physical principles of fluorescence and its impact on optical microscopy.

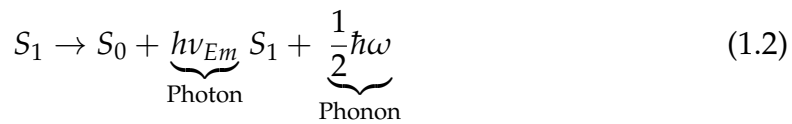
### 1.2.1 Fluorescence

Fluorescent molecules emit light at a longer wavelength than the incident photons. Fluorescence occurs when excited electrons (electrons not in the ground state) relax back to their ground state. This process is quantum mechanical whereby photons are emitted with energy equal to the energy of the difference of the ground and excited state [? ]. Fluorescently emitted photons will be of a lower energy and hence have a longer wavelength (**Stoke's Shift**). An excited electron will not typically excite to exactly the first excited state, but more likely a slightly higher degenerate energy state. From here the electrons will, over time "trickle" down to the lowest energy level available whilst emitting phonons (vibrational energy packets) until eventually they reach the first excited state ( $S_1$ ), relax and emit a fluorescent photon (see Equation (1.2)). Figure 1.1 demonstrates this excitation and emission process through the use of a **Jablonski diagram**.

#### Excitation



#### Emission



### Fluorescence Lifetime

Fluorescence lifetime is a valuable extra dimension of information exploited in biological imaging. The time an electron spends in the excited state will vary randomly but it will be governed by a probability; the longer the electron is in this high energy state the fewer electrons in a population will also be excited. If one were to excite a population of fluorescent molecules into an excited state the population

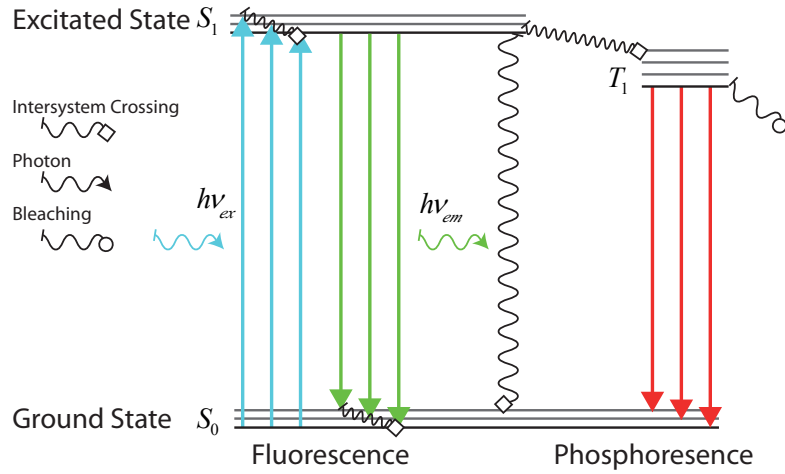


Fig. 1.1 Jablonski diagram representing in colour the excitation of Alexa Fluor<sup>©</sup> 488 in a standard two level fluorescent system.

would begin to decay with an associated time constant  $\tau$ , see Equation (1.3).  $Q_{21}$  is a non-radiative process that has a direct environmental dependence with an impact on  $\tau$ , as a result the decay constant can be affected (and therefore measure) by a multitude of factors including photochemistry, local viscosity [?], temperature [?], pH and more.

$$[S_1](t) = [S_1]_0 e^{-\frac{t}{\tau}} \quad (1.3)$$

where

$$\tau = \frac{1}{\underbrace{A_{21}}_{\text{Radiative}} + Q_{21}} \quad (1.4)$$

### Photo-bleaching

If a molecule for instance is excited to a singlet excited state  $[S_1]$  but decays atypically to a triplet state  $[T_1]$  photo-bleaching may occur, see Figure 1.1. In the triplet state the molecule is then susceptible to covalent reaction inhibiting the typical fluorescent reaction. Molecules in triplet states tend to also have longer lifetimes as the decay process from a triplet state is normally forbidden in terms of radiative decay. Explicitly for microscopy photo-bleaching is named fading as it literally means a sample that is imaged over an extended time will produce less fluorescent signal and fade.

## Photo-toxicity

As well as fluorophores photo-bleaching due to exposure, biological specimens can be overly exposed to light. Most biologicals are exposed to solar EM radiation regularly and most of those utilise it in some manner, as a result overly exposing a sample to photons can be toxic to them causing experimental complications and oddities in observed reactions or even death. A reasonable standard to consider as a "safe" exposure for a biological is that of the solar constant; it is a fair assumption that most biologicals are capable of surviving the Sun as they have evolved in that manner. The Sun has a solar constant of  $\sim 1 \text{ kW m}^{-2} = 1 \text{ nW } \mu\text{m}^{-2}$ , assuming 10 minutes of exposure is also safe that would imply an energy density of  $\sim 0.6 \mu\text{J m}^{-2}$ . A cell diameter is  $\sim 100 \mu\text{m}$  and an embryo diameter is  $\sim 900 \mu\text{m}$  meaning they should only be exposed to tens of millijoules and hundreds of millijoules respectively [? ].

### 1.2.2 Widefield Fluorescent Microscopy

The key concept behind the fluorescent microscope is the ability to separate excitation and emission. Classical optical microscopes as well as electron microscopes both had the problem of separating these signals. Non-fluorescent optical microscopy employed many techniques including dark field and phase contrast microscopy to avoid this problem, however they could not address it so fundamentally [? ]. Through fluorescence the signal retrieved from the sample is chromatically labelled. The invention of the dichroic mirror allowed these signals to be physically redirected and therefore detected completely independently. Excitation and emission filters are used to improve light source spectra and limit scattered light emissions, see Figure 1.2.

## Limitations

### The Point Spread Function

**Spatial resolution** is the ability of an observer to physically distinguish two close objects in an image [? ]. Wide-field microscopes are classically limited to 250 nm resolution as the wavelength of visible light is of this magnitude [? ]. Within a microscope the true limiter is the impulse response of a lens when passing light. A lens, when focussing and magnifying, can be thought of as a low pass filter; it

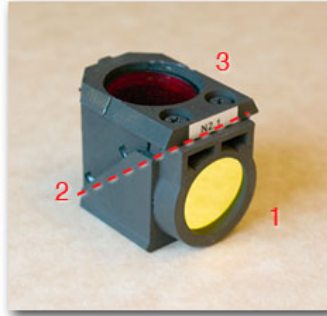


Fig. 1.2 Standard fluorescent filter cube. (1) Excitation filter (2) Dichroic mirror (3) Emission barrier

permits low resolution information up until a cut-off frequency. In the Fourier plane this filtering is a circle of radius:

$$k_r = n \frac{2NA}{\lambda} \quad (1.5)$$

The inverse transform of this frequency filtering produces the function convolved with the sample being imaged, the Point Spread Function. See Figure 1.4 for a graphical interpretation.

### The Rayleigh Limit

Lord Rayleigh appraised a limit of resolution in an optical system in terms of the separation of two Airy disc point spread functions. Rayleigh defined the limit as the distance when the maximum of the PSF is positioned on top of the first minima of the other. This definition implies a contrast between the two functions of 27%; if the intensity trough seen from two airy discs in a microscope is lower than that, then by Rayleigh's criterion (see Equation 1.6) the two objects cannot confidently be resolved, see Figure 1.3.

$$r = \frac{\lambda}{2nNA} = \frac{1}{k_r} \quad (1.6)$$

Non-optical far field techniques can resolve much smaller than the diffraction limit. However, each is limited in its biological imaging capacity. Electron microscopy uses electrons instead of photons to observe Angstrom sized particle [? ]. An electron

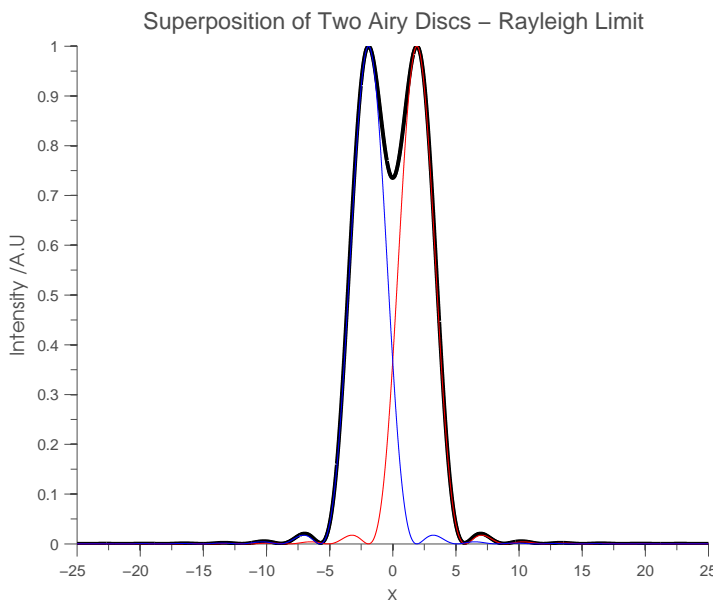


Fig. 1.3 Two identical objects separated such that they are "barely resolved", the contrast (intensity difference) between their superposition being 73% of the intensity maximum.

microscope is limited by its De Broglie wavelength, the effective size of an electron, on the pico meter scale [? ? ]. Electron microscopes are impractical for *in vivo* biological studies, as high intensity electron beams require conductive dissipater coatings which impede and damage biological processes.

Atomic force microscopes use sensitive piezo crystals to position and record surface information from samples using a cantilever at the nanometre scale [? ]. The tip of an AFM is convolved with the profile of the surface and so is limited in resolution to the size of an atom. Atomic force microscopes are slow raster scanning imaging techniques but more crucially offer no sample specificity, which is requisite to biology as it involves querying how two biological agents interact or how an agent acts in environment: e.g observing diseased cell interactions in a mouse brain model [? ], monitoring cancerous tumours [? ] and understanding virus structure [? ].

### 1.3 Three Dimensional Imaging in Life Sciences

Thick biological samples cannot be imaged well in classical optical microscopes. The depth of field of the point spread function and general occlusion caused by

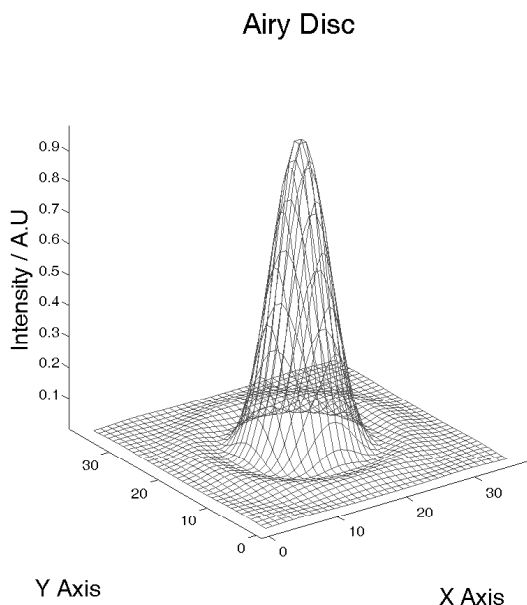


Fig. 1.4 Graphic representing the point spread function in arbitrary units of a lens. This function is convolved with any sample being imaged through its respective lens.

imaging through material meant that biologists would historically mechanically section their samples in preparation. Mechanical sectioning is highly invasive which is why Zsigmondy originally suggested (1912) the ultra-microscope as a way optically sectioning [? ]. This technique involved shining sunlight through a very narrow slit perpendicular to the optics of the microscope. Transmitted light microscopes relied on lighting beneath the sample and the eyepiece positioned above, this technique was proposed to alleviate out of focus light blurring the image of the sample. However, the difficulty and inherent mechanical issues of the technique meant that confocal microscopy by Marvin Minksy (1957) [? ] became the standard tool of biological imaging.

### 1.3.1 Confocal Microscopy

Confocal microscopy offers several advantages whilst also being entirely compatible with current fluorescent labelling techniques. By placing a small pin hole in the detector arm of a standard epi-fluorescent microscope, out of focus light from above and below the focal plane is rejected [? ], see Figure 1.5. This intrinsically allows

microscopy in three dimensions, in thick biological samples with an improved axial and lateral resolution improvement over wide-field [? ], see Figure 1.6. Confocal microscopy does have its disadvantages too; the pin hole in the detection arm means that the image needs to be constructed by raster scanning a point of light through a sample, which is slow. This can be achieved using a Nipkow disc or a pair of conventional galvanometer mirrors whose angle is dependent on input voltage. The use of this pin-hole has severe consequences in terms of photon efficiency. Firstly, the majority of the photons emitting from the sample are discarded, meaning that to get a good, high contrast image in a wide-field microscope will require a less intense light source. Secondly, as mentioned in Section 1.2.1 most confocal microscopes use light intensities in the “multiple-suns” regime [? ], which as discussed, is likely to be an unnatural level of exposure.

### Two Photon Microscopy (2P)

In confocal microscopy out of focus light is removed by using a pinhole in the focal plane; the fluorescent dye in the out of focus areas of the sample will still be exposed to this out of focus light and so photo bleaching still occurs but with there is better optical sectioning [? ]. Two photon microscopy optically sections by exploiting fluorophores which only emit when two photons are present for excitation, for this to occur the local photon density has to be high and so the focal point is the only place where fluorescent emission is likely to occur.

#### 1.3.2 Selective Plane Illumination Microscopy Principles

By using orthogonal illumination and detection (as in Figure 1.7) Selective Plane Illumination Microscopy is fast and less photo-toxic than confocal microscopy and two photon with only slightly lower lateral and axial resolution. A typical diode laser in a SPIM will supply up to 100 mW in a beam waist of  $3\text{ }\mu\text{m}$  with an area of  $\sim 7\text{ }\mu\text{m}^2$  which is  $\sim 14\text{ }\mu\text{W m}^{-2}$  meaning its toxicity is in that of the “single sun” regime. Depending on the field of view SPIM can be as little as 500 times faster than confocal as it does not need to acquire its signal by raster scanning, point-wise. SPIM has permitted the studies of *in vivo* whole samples typically for developmental biology [? ? ] with minimal photo-toxic repercussions. Its advantages have been successfully demonstrated where the several day development embryos of *Drosophila* [? ] and Zebrafish [? ] have been observed.

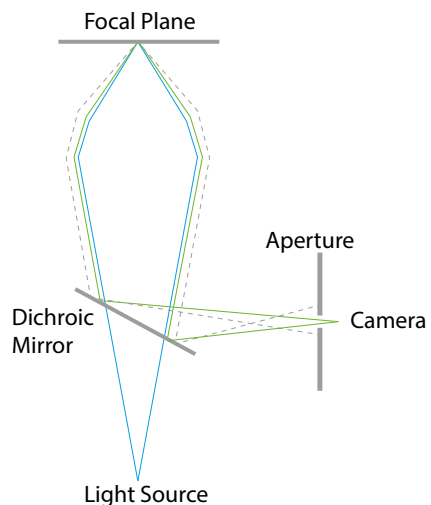


Fig. 1.5 Confocal microscopes reject out of focus light in the detection path, improving axial and lateral resolution for the sake of speed of image acquisition and photo-toxicity.

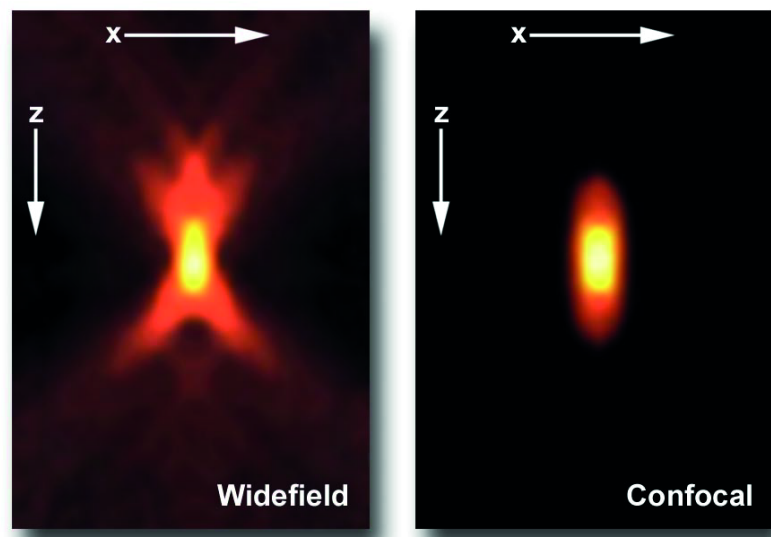


Fig. 1.6 Widefield versus confocal point spread function demonstrating axial and lateral resolution improvements [? ]

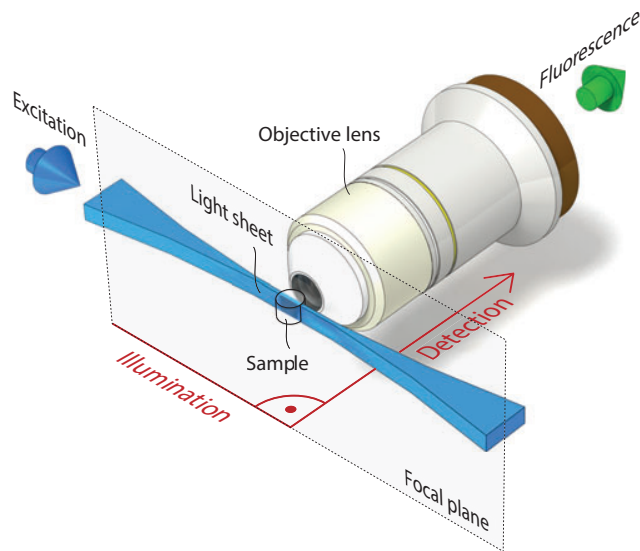


Fig. 1.7 Diagram demonstrating the geometrical configuration of illumination and objective [? ].

## Modalities

Orthogonal illumination can be created in two modalities. A cylindrical lens can be used to image a light source onto a sample as a thin sheet of light. **Digitally Scanned Light sheet Microscopy** uses galvanometer mirrors to rapidly scan a thin light source through a sample [? ]. Using cylindrical lenses to create a light sheet is implicitly faster than digitally scanned light sheets, however the bottleneck with each is due to the exposure time of the camera. A galvanometer mirror can oscillate at tens of kilohertz which is a hundred fold faster than typical sCMOS cameras can capture. The major advantage of a cylindrical lens is that it is cheaper and more easily aligned than its counterpart the galvanometer scan mirror, which is why projects like *OpenSPIM*<sup>1[? ? ]</sup> make use of cylindrical lenses to ensure SPIM is more available and affordable to lay builders and users. For the expense and technical ability needed for dLSM it does offer advantages such as better optical sectioning, a

<sup>1</sup>*OpenSPIM* is a project to bring affordable light sheet microscopy to scientists who have little or no experience with optics, engineering or hardware interfacing. Projects like this and *OpenSIM* ensure that the technology is freely available to benefit everyone so that biological and medical understanding can be furthered efficiently and universally.

more homogeneous field of view and crucially the ability to positively exploit effects of the system, such as confocal slit scanning.

### **Confocal Slit Scanning**

Confocal slit scanning is a technique which heavily exploits the scanning nature of dLSM. sCMOS cameras in SPIM systems expose all the pixels equally in a frame, a shutter then rolls exporting all the pixel values so that each pixel of the current frame is synchronised and the final image is not torn or sheared. Confocal slit scanning exposes several rows of camera pixels with roughly equal width to the scanning laser beam. This area of active pixels is rolled synchronously with the movement of the laser scanning. The result is a virtual slit that confocally improves the resolution and contrast of a captured image though potentially needing more photons to create an image of the same overall intensity [? ].

### **Non-Classical Illumination**

SPIM is fundamentally limited in terms of field of view and axial resolution when using classical illumination. A typical light sheet created using a cylindrical lens or virtually will have a beam waist, a section along the propagating wave where its thickness is its smallest. As such, light used to optically section a sample will not propagate uniformly and this thickness expands more steeply the narrower the beam waist is [? ]. Betzig et al demonstrated very successfully how Bessel beam illumination can be exploited. By creating an annular ring of light in the Fourier plane a narrow propagating and self reconstructing light sheet can be produced [? ]. Crucially the beam waist and extension of this type of illumination profile has no dependence, so the field of view homogeneity can be maintained whilst squeezing the light sheet to a diffraction limited thickness. Bessel beams can be created online using spatial light modulators, as well as offline using phase masks.

### **Spatial Light Modulators**

A Spatial Light Modulator is a digitally addressable two dimensional surface which can control either phase or intensity of incident light at any of its pixels. To this end one can create dynamic structure in illumination, which would be very difficult classically. The pixel nature of an SLM means that the reflected light will suffer from artefactual noise. To correct for this, incident light impinges the SLM

at a shallow angle (to ensure the image is not sheared, Hamamatsu recommends a maximum 5° angle) where the exit light does not follow the optical path through the remainder of the system. Instead this “zero order” light is absorbed by a beam block, and the desired modified wave front is steered using a projection on the SLM.

Not any phase or intensity pattern can be projected either, each pixel will have a limited pitch with quantised steps through its dynamic range. This means that if two neighbouring pixels need very large phase differences compared to the full dynamic range, sample issues may cause incident light to behave unpredictably.

SLMs are typically made using liquid crystals, nematic or ferroelectric. Ferroelectric liquid crystals are very fast (~500 Hz [? ]) but are limited to binary phase or intensity. Nematic liquid crystals can rotate proportionate to electric field voltage allowing continuous phase modulation but are slow in comparison (~60 Hz [? ]). Liquid crystals can also suffer photo damage, though advances in coating technology and liquid crystal chemistry have set the intensity damage threshold to limits outside of those used by visible light microscopy; liquid crystals however are still susceptible to light with wavelengths outside of typical operations. Wavelengths below 400 nm being damaging for Hamamatsu’s SLMs for instance [? ].

### Tunable Lens Scanning

A tunable lens is a device which can perturb the focus of a deformable lens, usually liquid (deformed by electro-wetting) or plastic (mechanical deformation). The change in lens curvature affects the focal length of the tunable lens. Using a pair of tunable lenses allows sufficient degrees of freedom to be able to control both the position and extension of the light sheet independently. Changing the focal length of the lenses so that the light is collimated but the magnification of the excitation beam at the back aperture (which controls the NA) of the objective is larger, this will extend the beam (increasing the beam waist), whilst changing the focal lengths (so that the excitation light at the back aperture is convergent or divergent) will reposition the beam waist of the light sheet further away or closer to the objective [? ].

This level of fine control enables one to circumvent the typical trade off between light sheet extension and thickness. By stitching several thin light sheet images obtained at different depths in the sample, creates an overall higher resolution image for the sacrifice of speed and photo-toxicity. Changing the position of the light sheet (when its extension is short) as it is scanned through the sample means one can *bend*

the light sheet around an area of interest, increasing resolution of key components of a sample and greatly reducing overall photo-toxic effects.

## 1.4 Particle Tracking In Life Science

Particle tracking is a relatively young but vital tool in modern quantitative biology and the field of bio-informatics. A particle can refer to anything that is particulate and is not exclusively large or small, circular or spherical etc. These techniques are very useful at numerically quantifying and detecting large population movements to discern general trends. For instance, pollen grain diffusion; a singular grain of pollen will be erratic and random whereas several hundred recorded paths will reveal a general diffusive trend through averaging. Particle tracking lends itself very heavily to the study of intracellular dynamics, answering important biological questions such as: viral infection movement [? ], intracellular membrane dynamics [? ], genome maintenance, gene transcript [? ] and more [? ].

Particle tracking using light sheet microscopy is very relevant due to the high imaging speeds required to study particles that are both small and fast. Confocal microscopes suffer because they cannot temporally resolve particles; widefield microscopes suffer because they cannot provide three dimensional data; SPIM can offer both.

### 1.4.1 Particle Spatial Localisation

Particle tracking can be broadly described as a two stage process. Spatial localisation then temporal localisation. The spatial localisation of a particle involves accurately marking where one or many particles are within an image. Humans are naturally able to do this as they have evolved to notice patterns and anomalies. Programming a computer to undertake this exercise was an early feat in the field of computer vision [? ]. Crocker et al deconstructed the problem into logical computable steps.

Firstly Crocker's data was deconstructed as singular images in two dimensions rather than full video volumetric data. Secondly each image was corrected for any distortion or error as digitised video is inherently imperfect and may not be truly representative. Each image has a threshold found from an estimate of the

background value of the image. This threshold removes substantial noise that would otherwise contribute to the final result. Pixels with local maximum brightness are identified as “candidate” particles and compete with other candidates within a pre-defined radius slightly larger than the expected size of the particle.<sup>2</sup>

A centroid (centre of mass) fitting procedure is employed under the assumption that, to a first order approximation, spherical scattering emitters can be well-defined by a Gaussian profile. By fitting a Gaussian profile and using tens of pixels to minimise error, particulate positioning can be defined to sub-pixel accuracy. The most common method of Gaussian fitting due to its ease of implementation, speed, precision and robustness is iterative least squares fitting.

### Overlap

It should be noted that an obvious flaw with Crocker’s method is that it does not account for overlapping particles. This problem is apparent in dense particulate systems; experimental and computational methods are addressing this [?], but for the most part these cases are marked as rare outliers and typically rejected in particle tracking routines as samples are usually constructed with a sensible sparsity.

### 1.4.2 Particle Temporal Localisation

When localising particles temporally, images of particle distributions need to be taken swiftly enough so that any change in particle position is small enough such that it can be judged as the same particle but in a different position at a time later, *beyond reasonable doubt*. Computationally this is achieved by assigning a global cost metric to the distance between particles which is then minimised to find the most likely solution of how particles in the first image have translated into the second image.

### 1.4.3 Single Particle Tracking

Tracking individual particles is an important tool for modern biology. It has been used to study virus trafficking and how viruses penetrate the nucleus of a cell [?];

---

<sup>2</sup>Methods since Crocker for a truly blind particle recognition have since been proposed but Crocker serves as a poignant historical but still relevant method of particle tracking using Computer Vision

intracellular transport such as the movement of mRNA [? ]; cell membrane dynamics [? ] and more.

### **Light sheet single particle tracking**

A very novel and exclusive way of full three dimensional particle tracking using SPIM has been proposed. By using a static lightsheet and an XYZ translator one can move a particle back into the FOV laterally if it drifts. Once the particle is re-localised, the encoded position on the z aspect of the stage is then equal to the position of the axial position of the particle by virtue of the repositioning. The x and y position are then derived using Crocker's centroid fitting from the resulting image accurately in post processing.

This method vastly improves the lateral resolution of the SPIM system as well. Volumetric methods would limit the lateral resolution to half the beam waist,  $\sim 1\mu m$ , whereas this method is exclusively limited by the step size of the z translator (which can be very high resolution when using piezoelectric crystals) and one's ability to ensure the particle is precisely central within the excitation laser (which is then dependent on the particle size). Spille demonstrated this technique very successfully on a single molecule of mRNA ( $50nm$  [? ]) moving on the membrane of a nucleus [? ]. SPIM's speed makes the technique very enticing as it is unrivalled for the purposes of particle tracking. See Figure 1.8.

This method could then be further improved using a tunable lens excitation, by tracking the position of the particle in x using the tunable lens and y by narrowing the trace of the scan mirror, the temporal and spatial resolution of single particle tracking could be vastly improved yet again. Z position information could also be encoded into the image by virtue of light beam intensity. By ensuring the particle is limited to half of the beam profile of the light sheet, then intensity of the particle would be proportional to a Gaussian curve z position. This method could prove to be faster, more accurate and less perturbing on the sample as mechanical motion would be removed.

### **Remote Focusing**

There are three ways in which to realise the full three dimensional SPIM. The simplest way is to move the sample through the light sheet as is done in Oblique Plane Imaging. The second method involves scanning the light sheet through z

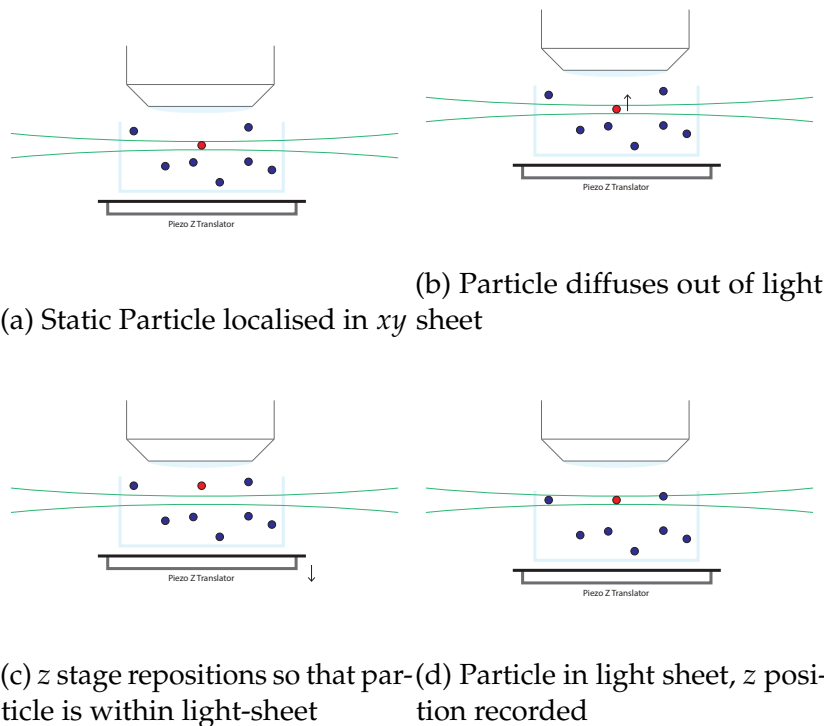


Fig. 1.8 Routine to track particles three dimensionally in SPIM

which is potentially faster; the issue which then arises is that the light sheet moves out of the focal plane of the detection objective. The focal plane can be moved onto the light sheet by moving the excitation objective, however this method (like the first method) causes perturbations to the sample. Huisken et al offer an alternative where the focal length of the objective is adjusted by placing a tunable lens in the detection path (similar to section 1.3.2)[? ]. Huisken shows using a contrast grid that image quality and aberrations are negligibly affect and goes on to produce 100 Hz volumetric imaging though on small volumes [? ].

## 1.5 Technologically limited Biological Questions

### 1.5.1 Neuro-degenerative Disease

Current Alzheimer's disease models suggest that Amyloid beta fibrils elongate creating Amyloid plaques. These plaques then pathologically cause an over production of tau in the first affected neuron. This over production in the first neuron quickly produces toxic levels of tau which propagate into neighbouring neurons, causing a cascade neuronal degeneration [? ].

Mechanisms for AD are not fully understood but tau protein misfolding is expected to play a role in the pathology[? ]. Our group has shown that extracellular tau proteins cause the endogenous over-production of tau proteins [? ]. The group has begun to observe tau propagation in axons two dimensionally. Observing the movement of tau proteins between neurons three dimensionally would perhaps reveal the mechanisms by which tau pathology neurodegeneration occurs, more specifically how extracellular tau proteins originated. It is hypothesised that stress impact may be a cause of the secretion of tau proteins causing the degeneration of other neurons [? ? ]. An *in vivo* study in a live animal model being impacted could verify this using light sheet particulate tracking.

It is possible that tau proteins move too quickly to be successfully tracked. In our group Tau proteins have been monitored to move between neurons via axons at a rate of 480  $\mu\text{m}$  per 20 minutes or 0.4  $\mu\text{m}$  per second. A standard confocal image exposure is on the order of 2 to 3 seconds, meaning a tau protein could displace during the image acquisition by 1.2  $\mu\text{m}$ . This movement during exposure could lead to a tau protein appearing to be of the order microns, whereas in fact it is of the order tens of nanometres. Light sheet technology can image 300 times faster and so a

propagating tau protein would only move 4 nm during an acquisition, less than the size of the protein and so an acceptable error. Most importantly, tau is of comparable size to mRNA which has already been successfully tracked within a live cell using light sheet SPT [? ].

### 1.5.2 Virus Trafficking

Virus particles are of the same length scale as mRNA and tau proteins and so can also be tracked using light sheet SPT. Viruses reproduce by exploiting cell structure. A virus particle will interact with the cell membrane either singularly or in a plaque to release the contents of the virus inside the cell. Proteins are released to suppress the immuno-response and enable suitable conditions for the viral genome move into the cell. Once inside, the virus moves to areas within the cytoplasm or nucleus and begins replication. Replicated viroids then leave the cell and the cycle continues. Individual virus particles may follow a multitude of different paths or even fails completely during infection. By tracking viral infection at the single virus level observers can deconstruct the dynamics of virus-cell interactions.

There are several challenges in tracking virus particles. Firstly, viruses are small, varying from 20 to 200 nm, sub-diffraction limit. Virus labelling is also difficult due to its size and nature. Fluorescent probes are comparable to the size of the virus and so can hinder infectivity. Proximity of the fluorescent probes due to virus size can also cause self-quenching within the probes [? ]. Furthermore less than 1 % of virus particles successfully reach the replication stage. Some viruses for instance require large plaques to breach a cell membrane. Finally a live tissue study is desirable in modern biology [? ] which is logically challenging in terms of mounting and ample preparation.

Light sheet particle tracking can produce sub-diffraction limit 100 Hz video, resolution sufficient to watch virus particles *in vivo*. Due to the low photo-toxicity of light sheet, multiple virus particles could be tracked concurrently without damaging the cell compared to confocal techniques. Light sheet has been used successfully on live tissue, in live animal models [? ] and importantly light sheet SPT has been used in a live cell [? ]. Light sheet particle tracking is by virtue three dimensional and *in vivo* allowing an unprecedented level of detail in a viral study using this technique [? ].

# Chapter 2

## Contemporary light-sheet technology

Light sheet fluorescence microscopy (LSFM) is revolutionising the way in which complex, living biological samples can be imaged at high spatial and temporal resolution. The technique deviates from conventional epi-fluorescence microscopy in that one illuminates the sample orthogonally to its detection. The decoupling of illumination and excitation allows for the construction of light sheets whereby a single plane of interest is excited. As such the technique offers optical sectioning capability comparable to a confocal microscope whilst still using a wide field detection system [1–3]. This garners two key advantages: firstly, as the plane of interest being detected is irradiated, the incident photon dosage is drastically reduced and so photo-toxicity to the sample is minimised. This is in stark contrast to confocal imaging where signal is collected from a small voxel along the illumination axis whilst the entire sample is illuminated when recording a single image plane. Secondly, wide field detection enables a significant temporal resolution increase in LSFM versus confocal. For rapid volumetric imaging of complex organisms LSFM is becoming the technique of choice in developmental biology [4–9], plant science [10] and cell biology [11, 12].

The concept of orthogonal detection and illuminations dates back to 1903 when Zsigmondy and Siedentopf studied colloids in their *Ultra-microscope*. Technological advances in fluorescent dyes, labelling and digital image detection has permitted Voie *et al* [2] to present the first light sheet fluorescence microscope in 1993. By 2004 Huisken *et al* [3] demonstrated the potential of LSFM for *in-vivo* imaging with cellular resolution. Their Selective Plane Illumination Microscope (SPIM), seeded a

rapid development in the LSFM field and is chosen here as an example to discuss the main concepts of LSFM.<sup>1</sup>

## 2.1 Generating Light Sheets

- ✓ Optically
- ✓ Virtually
- ✓ Volumetric Imaging

### 2.1.1 Light sheet generation

#### 2.1.2 Optical Light sheet Generation

Huisken *et al* seminally used Gaussian laser emissions for the generation of their light sheets despite Gaussian beams have a distinct trade-off when used in LSFM applications, in that the thinner the light sheet the narrower the usable field of view. Equation (2.1) models the Gaussian beam approximation where the full-width half-maximum ( $\sqrt{\ln(2)}\omega(z)$ ) increases as a Lorentzian when a distance  $z$  away from the focal plane (Equation (2.2)). The rate at which this occurs is dependent on the Rayleigh length in Equation (2.3) which quantifies the trade-off. The confocal parameter ( $b = 2z_R$ ) is a metric for the distance over which a Gaussian beam propagates as if it were parallel (neither converging nor diverging). For LSFM this is the distance over which the light sheet can be assumed to be of homogeneous thickness.

Huisken also pioneered the use of a cylindrical lens to focus the Gaussian beam one dimensionally into a Gaussian light sheet. The Gaussian nature of a beam's intensity for LSFM requires that the excitation beam is over expanded and later cropped by an aperture to create homogeneous illumination. The procedure is optically lossy, but, laser intensity is typically in surplus for fluorescence microscopy techniques; a typical fluorescent sample needs  $2 \pm 1.5$  mW versus a low end diode laser emitting 100 mW+.

---

<sup>1</sup>Design choices made here have heavily influenced the openSPIM project, an information toolkit found on the internet for constructing a LSFM

$$I(r, z) = I_0 \left( \frac{\omega_0}{\omega(z)} \right)^2 e^{\frac{-2r^2}{\omega(z)^2}} \quad (2.1)$$

$$\omega(z) = \omega_0 \sqrt{1 + \frac{z}{z_R}} \quad (2.2)$$

$$z_R = \frac{\pi \omega_0^2}{\lambda} \quad (2.3)$$

Where:

$z_R$  is the Rayleigh Length

$\omega_0$  is the spot of size of the beam.

$\lambda$  is the wavelength of light.

### 2.1.3 Digital Light sheet Generation

Keller *et al* [13] proposed sweeping a narrow laser beam through the sample to create a virtual light sheet. This was achieved by oscillating galvanic mirrors at kHz frequencies, well over the Nyquist limit in comparison to the imaging acquisition rate [13]. To ensure a homogeneous illumination and distributed photon dosage a tele-centric  $f\theta$  lens was used to convert beam angle optically from the scanning mirrors in to a linear position <sup>2</sup>.

Using DSLM instead of a cylindrical lens based system offers some key advantages. Firstly, as the beam is scanned rather than stretched there can be no optical interference of coherent photons between neighboring regions, this reduces speckles and shadows. Secondly, illumination intensity can be modulated such that structure can be superimposed on the sample giving the potential for super-resolution image improvement. This resolution improvement has so far solely been experimentally demonstrated in the direction of the the scanning due to geometrical constraints [14].

### 2.1.4 Volumetric imaging

The true power of light sheet microscopy becomes evident in its fast volumetric imaging capability. Huisken's original SPIM required samples to be mechanically scanned through the static light sheet, potentially disturbing the sample depending

---

<sup>2</sup>A practice borrowed from laser scanning microscopy.

on the speed of the scanning. dSLM has the potential to subvert the static light sheet by using a second galvanometric mirror to move the light sheet relative to the static sample, the detection objective is then mounted on a high speed and precision axial translator and tuned to follow the light sheet. Ideally piezoelectric actuators are used as their settling times are on the order of milliseconds providing speed and accuracy needed to match 100Hz cameras. Of course, with dSLM, instead of the sample motion causing a disturbance a large objective local to the specimen is causing turbulence. This was matched optically through the use of an electrically tunable lens [15] that moves working distance of the detection objective. This technique suffers from: fluorescent signal losses in the further four lenses and two mirror surfaces<sup>3</sup> ( $\sim 80$  percent signal retrieved); spherical aberration and is a more involved method as the system requires a non-linear calibration.

## 2.2 Objective Arrangements

### 2.2.1 Single View

Light-sheet microscopes are distinct in that two objectives are used orthogonally causing the technique to incompatible with most standard epi-fluorescent biological mounting practices. Efforts have been made to make light sheet imaging more accepted through novel objective arrangements as well as new and intuitive mounting approaches.

#### Horizontal Orientation

- ✓ Flat (openSPIM) open-SPIN diy-SPIM
- ✓ MuVIEW[16]
- ✓ Vert
- ✓ V (diSPIM)
- ✓ 60/30 Lattice Light Sheet and Objective Compatibility (Short section)

#### Multi VIEW

---

<sup>3</sup>The mirrors are used to ensure the ETL is horizontal to gravity as further aberrations occur if the tunable surface is not entirely flat. In essence two mirrors from the tunable light sheet could be removed by using mechanically deforming tunable lenses instead of electro wetting tunable lenses.

Huisken *et al.*, for instance, used two objectives in a horizontal configuration with a detection objective built into the sample chamber whilst the illuminating through a clear window. This configuration was chosen so that a sample could be lowered into the system and, crucially, rotated without gravity causing registration errors when reconstructing the volume tomographically. Rotational volumetric imaging also minimises shadows and improves image quality lost to scattering especially in thick ( $>500\mu m$ ) samples. Mounting a sample from below and rotating produces the same result but requires a more sophisticated chamber design to contain the sample medium. A horizontal geometry is vital also for plant biology as the objectives do not inhibit the plant's natural tendency to be upright [10].

### **Vertical Orientation**

An alternative to the Huisken's horizontal configuration is positioning the detection objective above the sample and illuminating from the side. A vertical orientation is an attractive option as it can be compatible with commercial optical microscopes as well the chamber not requiring an inbuilt detection objective. Both of these techniques can allow at additional illumination objective, by offsetting the foci of the illumination objectives an overall more homogenous field of view can be created.

### **(45<sup>o</sup> Orientation)**

Shroff *et al* then pioneered use of two objectives in a V configuration above the sample through iSPIM. With choice objectives, adhered samples prepared with standard mounting procedures can be imaged in a petri-dish [17].

### **Optimal Orientation**

In a bid to maximise sample accessibility and numerical aperture, Betzig *et al.* [14] commissioned a high NA (0.6) custom excitation objective to fit with their high NA (1.1) detection objective (Nikon CFI75). In mounting the orthogonal pair at an angle such that they were flush so a flat surface, Betzig *et al.* created the most unhindered sample mounting conditions realistically feasible using two objectives. Tricks to circumvent objectives interfering with sample mounting are needed as high NA objectives are physically large. Moreover, high NA objectives typically have short working distances and require both objectives to be close, and likely cause spacial

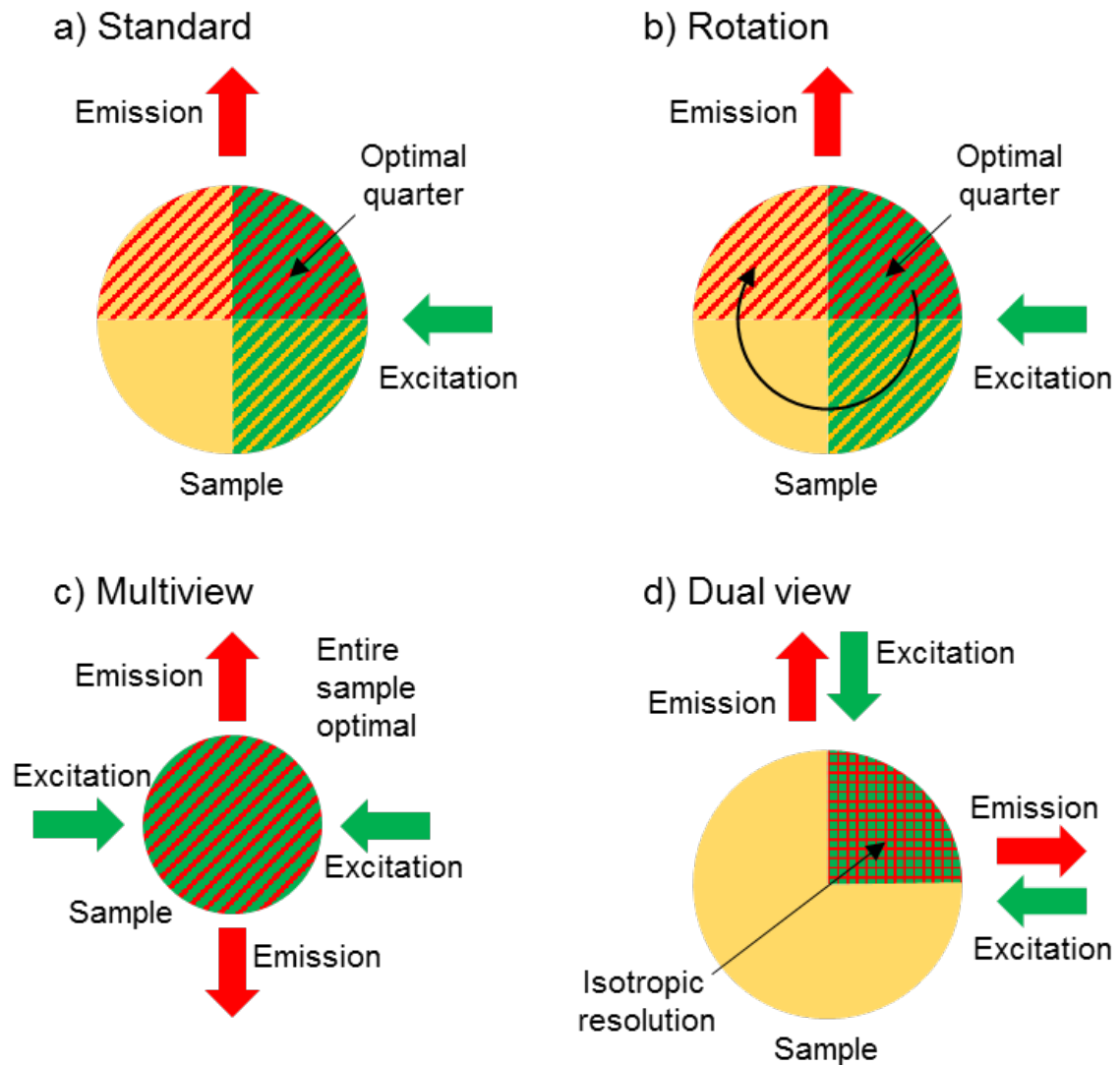


Fig. 2.1 (a): The simple SPIM field of view – only a quarter of a sample has optimum illumination (green) and excitation (red). (b): by rotating a sample field of view can be quadrupled but at a cost in acquisition time. (c): By adding extra excitation and detection path the entire sample can be imaged without a rotation. (d): by making optical paths of a LSFM dual purpose a quadrant of a sample can be imaged from two orthogonal perspective and with correct image fusion achieve isotropic resolution. tod

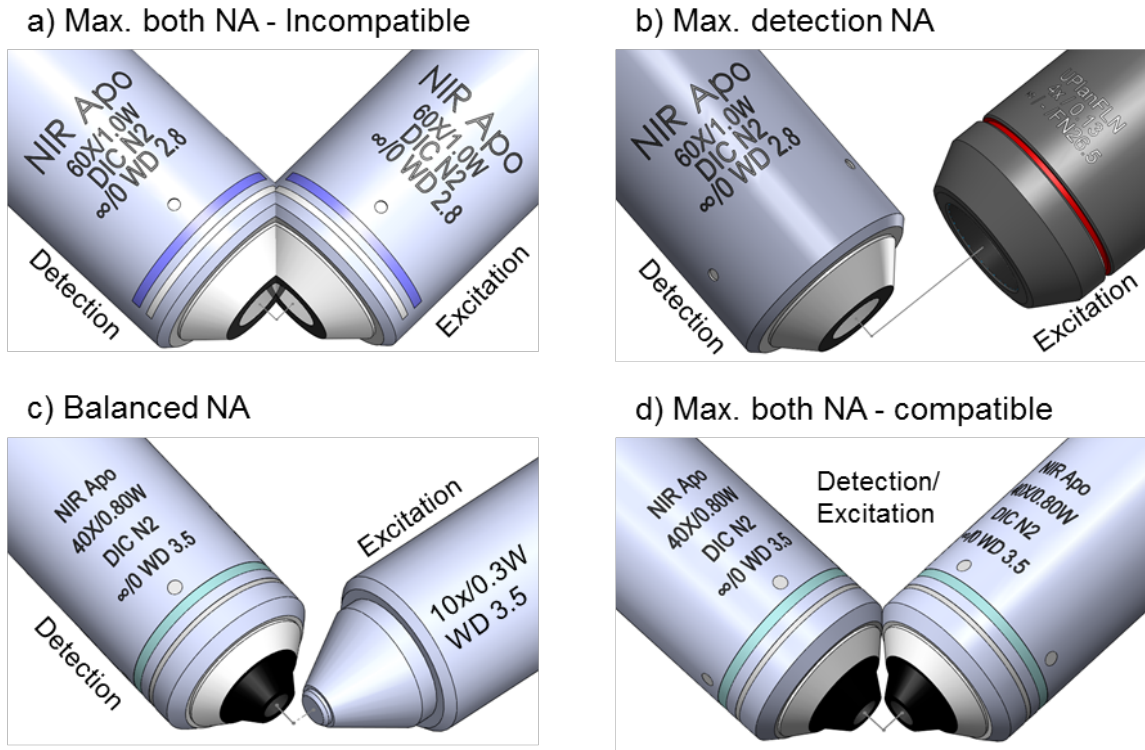


Fig. 2.2

incompatibilities even with the narrowest excitation objectives. See figure ?? for a detailed comparison.

## 2.2.2 Multi-View

Shroff *et al* introduced alternately imaging between each objective of the iSPIM in the form of the diSPIM [17].<sup>4</sup> Axial resolution that would otherwise be lost to thick light sheets is recovered by switching the imaging and detection arms. The two data sets captured by each camera are fused in post processing to provide near isotropic three dimensional resolution. Where LSFM provides the most improvement over other techniques, such as in large, thick biological samples , scattering becomes significant both for excitation and emission light. diSPIM however does not address inherent issues of scattering in thick samples, there is an *optimal quarter* (see Figure 2.1) wherein excitation and emission photons are the least scattered.

<sup>4</sup>This system is now a commercial light sheet solution provided by ASI.

Krzic *et al* returned to the horizontal orientation of Huisken's SPIM, and chose their objectives wisely in MuVU-SPIM where two excitation and two detection objectives were packed around a hanging sample. MuVu can reach all regions of its sample, but it cannot dodge scattering limitations homogeneously. To minimise gross scattering, sample rotation is necessary, of course acquiring volumes tomographically raises its own unique issues such as volume registration, rotational synchronisation and lengthy acquisition times. Regardless, for large samples two objectives in Huisken's original SPIM provide a cost effective robust volumetric imaging solution; with projects like the OpenSPIM have received significant acceptance and community attention.

## 2.3 Single Objective Light Sheet Microscopy

- ✓ Axial Plane [18]
- ✓ Oblique Plane [19]
- ✓ Fibre SPIM [20]
- ✓ Mirrored Cuvette,
- ✓ Confocal adaptor

Prior to refinements in objective positioning Dunsby conceptualised a system for single objective light sheet microscopy. The advent of such systems could provide a plug-and-play light sheet experience on commercial microscope frames. Dunsby proposed illuminating the sample using a high NA objective whereby the light sheet would illuminate at an oblique angle to the optical axis, the detected signal is then retrieved using the same objective [19]. Optically the sample is conjugated to a virtual position where a pair of objectives (excitation and detection) analyse the virtual sample in a conventional light sheet manner. The technique suffers from optical technology, only when using a high NA objective can the system fully capture detection perpendicular to excitation. Unfortunately, OPM is an involved technique as it requires that a standard light sheet microscope is constructed behind a further optical relay system.

Virtual sample manipulation is alluring as one can perform virtual manipulations that are physically impossible. Zhang *et al* [18] created their virtual sample using

a similar relay system to Dunksby *et al.*, but crucially they positioned an atomically flat mirror which precisely rotated their virtual sample by  $90^\circ$ . In doing so they could illuminate the real sample along the optical axis and their virtual projection from the mirror was imaged directly onto a camera using a standard wide field configuration.

Using small mirrors near the sample is another viable, though more restrictive, approach to single objective LSFM. Galland *et al.* fabricated micro-wells with  $45^\circ$  micro-mirrors [21], converting any commercial scanning microscope into a light sheet microscope. Leica produce a similar solution in the form of an objective adapter which holds two mirrored surfaces near the sample creating a similar effect. Both techniques limit the size of the sample and their sectioning capability heavily depends on the quality of the mirrors used.

Ploschner *et al.* attempted to minimise the size of the second objective rather than remove it. By substituting the second objective for a multimode fibre [20] not only could they provide more access to their samples, but they could also embed their excitation source into their imaging chamber. Assuming that a multi-mode fibre operates deterministically on an input light source, they were able to correct for the fibre using an SLM and further demonstrated the system's ability to produce exotic beam profiles.

## 2.4 Illumination

### 2.4.1 Gaussian Techniques

Illumination techniques have been proposed in a bid to circumvent the ubiquitous Gaussian beam extension versus thickness trade-off. The most intuitive approach is accepting the loss of FOV produced by Gaussian illumination and moving the focus of this strip of high axial resolution light to different parts of the sample. A final image can then be fused to achieve maximum axial resolution though with a direct cost for time of acquisition and photobleaching versus axial resolution, with an exceptionally high NA light sheet tending to become as slow and damaging as a confocal system .

CITE Variable light-sheet.

Fu *et al.* proposed tiling multiple thin Gaussian light-sheets that are focally offset to create a similar tiling effect without the temporal loss [22]. This effect was

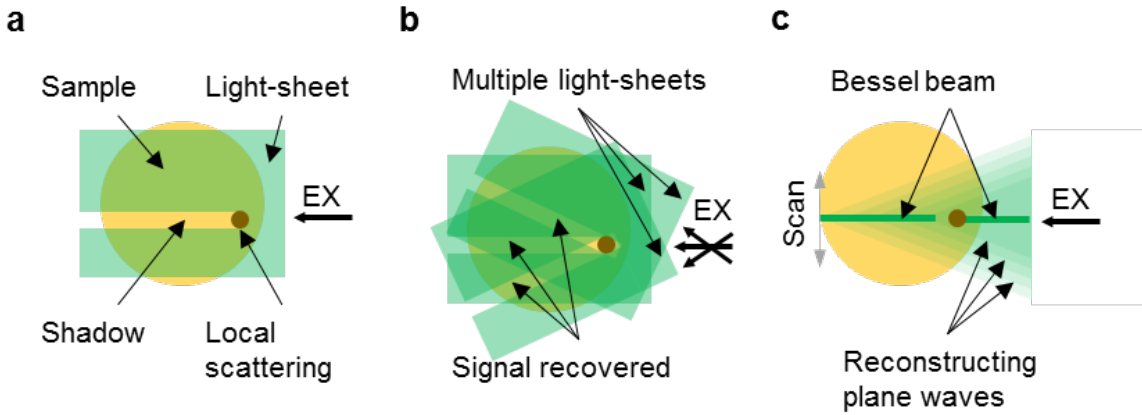
produced by using a Spatial Light Modulator whose hologram had superposed lens-like phase patterns superimposed. This technique again suffers from the additional photo-dosage imparted by the undesirable lobes of the Gaussian beam, moreover these low resolution sections also contribute to fluorescent background reducing the net SNR of the system.

### 2.4.2 Exotic Beams

Species of exotic beam do exist which do not subscribe to classical Gaussian beam limitations. Bessel beams are non-diffracting and self healing, meaning they reconstruct behind occlusions making them very desirable for light-sheet applications. They can be optically constructed from either an axicon lens or a amplitude mask with a annual ring opening, the latter being inexpensive but the most optically lossy. Unlike Gaussian optics their extension and thickness can be theoretically entirely decoupled, in practice a Bessel-Gauss beam only behaves over short distances [23] of up to  $\sim 30\mu\text{m}$ . Bessel beams however suffer from having multiple undesirable orders, the more ideal a Bessel beam is the more intensity is retained in its outer rings. As such a singular scanned Bessel beam itself causes a significant background. Betzig *et al.*[14] exploited these additional orders, they constructed multiple Bessel beams in the scanning plane by superimposing a sinusoidal amplitude pattern on to an annular amplitude mask. In doing so their undesirable orders constructed to reinforce the zeroth orders of the parallel beams. Finally they adjusted their now lattice light-sheet such that the outer orders above and below the scanning plane lay at minima in the detection point spread function reducing the net fluorescent axial background.

### Airy Beams

Airy beams also self-heal similarly to Bessel beams but comparatively are more extended. They are constructed using a coma-like phase pattern and exhibit characteristic a beam curvature. Though they extend several fold further than Bessel beams, their curvature produces an asymmetric profile along the detection axis. This is then required to be deconvolved in post processing. Vettenburg *et al*[24] demonstrated similar axial resolution improvement to Bessel beams whilst achieving a  $\sim 3$  increase in field of view.



### 2.4.3 Thinner Beams

Attempts to quantum mechanically narrow Gaussian Light sheets include using stimulated emission depletion and two photon emission (2P). Using an addition laser to deplete, through stimulated emission (STED), out of plane fluorescence can narrow a Gaussian light sheet to  $< 1\mu m$  [25]. Two photon light sheet microscopy requires an excitation from two concomitant photons of cumulative energy sufficient bridge the required energy gap. This requirement ensures that such excitation events are sufficiently rare and only occur where photon density is high. In epi-fluorescent microscopes this occurs in the focal plane with the probability reducing quadratically along the imaging axis. In light sheet microscopes this occurs at the axial centre of the light sheet making it much thinner than a comparable 1P excitation sheet.



# **Chapter 3**

## **Homographically generated light-sheets**

Light-sheet fluorescence microscopy is fast becoming the method of choice for imaging large volumetric samples. Optical sectioning of volumes can be achieved either by using a confocal pinhole to reject out-of-focus light or by illuminating orthogonally with a thin light-sheet. As light-sheet imaging is a wide-field technique, the temporal resolution is much higher than achievable via confocal scanning and the photon-dosage for generating an equally bright image is  $\sim 2$  orders of magnitude lower. This makes light-sheet microscopy ideal for imaging live biological specimens[3]. Commercial and home-built[26] light-sheet systems typically use a cylindrical lens to convert a circular Gaussian laser beam into a thin sheet. Alternatively, galvanometric mirrors can mimic this effect mechanically by rapidly dithering a laser beam; this is digitally scanned light-sheet microscopy (DSLM)[27]. Using galvanometric mirror pairs enables fast sweeping of the light-sheet through a static specimen. However, the use of a scan lens can lead to registration errors of the sheet with respect to the imaging plane, leading to an excess background fluorescence in large volumes. Here we compare nonlinear and linear methods for registering the stack excitation and imaging planes in a DSLM system.

### **3.0.1 Affine region of interest**

Aligning a digitally scanned light-sheet to a detection plane requires generating a control signal ( $V_x, V_z$ ) for the scanning mirrors. In two dimensions the  $x$  mirror extrema map to the edges of the imaging-FOV (field of view) and a linear ramp

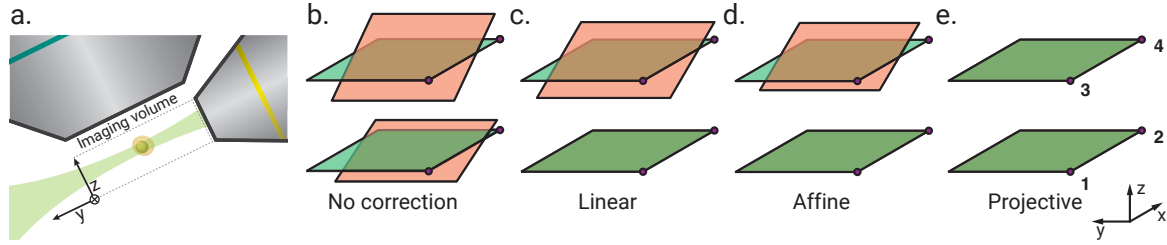


Fig. 3.1 (a) Schematic of the light-sheet optics using a large NA detection objective, the beam is scanned in  $x$  to create a virtual sheet. (b-e) For best image quality, the illumination planes (shown as red when not perfectly registered to the detection planes (green). The linear registration (c) tends to produce non-uniform out of focus illumination across the image. The affine registration (d) is commonly used to match the image centres between the top and bottom planes however the projective registration (e) for four control points provides superior performance due to decreased out-of-focus fluorescence.

between these coordinates produces a virtual light-sheet. The  $z$ -mirror extrema correspond to the top and bottom observed image planes. However, using linear ramping from a starting point, only three of the four  $x z$  extrema can be registered [28]. The fourth point is either discarded, or more typically, only the centre of the one of the axial planes is considered, essentially averaging the third and forth available vertices. As illustrated in Figure 3.1, this assumption then leads to a poorly-registered illumination in the plane where the fourth coordinate was neglected and greater background fluorescence in 3D imaging.

### 3.0.2 Projective region of interest

The stack of illumination planes used in a 3D observation can be better matched to the detection planes by registering four corners of the available excitation 3D-FOV, using a projective transform. Projective transforms can map any quadrilateral onto any other, whereas an affine transformation can only register 3 points. Higher order corrections could also be used, with an  $n$ -point correction using b-splines being one, computationally expensive option. However, such elastic transforms require more correspondences and are likely to incur additional errors through correspondence localisation precision.

### 3.0.3 Homography and homogenous coordinates

A calibration experiment provides the control signals  $(V_{x_i}, V_{z_i})$  for  $i = 1$  to  $4$ , needed to register the illumination to the four extrema of the imaging volume,  $(x_i, z_i)$ . In a projective transform of  $\mathbf{r}$ , we generate the augmented vector  $\tilde{\mathbf{r}} = (x, z, 1)$  and then apply a linear transform to obtain  $\tilde{\mathbf{r}}' = \mathbf{H}\tilde{\mathbf{r}}$ , followed by descaling to obtain the transformed vector

$$\mathbf{r}' = \begin{pmatrix} \tilde{r}_1' & \tilde{r}_2' \\ \tilde{r}_3' & \tilde{r}_3' \end{pmatrix} \quad (3.1)$$

A projective transform of a plane can be exactly defined by four projected points, unless any three are collinear. Now, the calibration experiment identifies four (non-collinear) extrema of the imaging volume, and so it is possible to combine the augmented form of three of the positions to produce the fourth, such that

$$\lambda \begin{pmatrix} x_1 \\ z_1 \\ 1 \end{pmatrix} + \mu \begin{pmatrix} x_2 \\ z_2 \\ 1 \end{pmatrix} + \nu \begin{pmatrix} x_3 \\ z_3 \\ 1 \end{pmatrix} = \begin{pmatrix} x_4 \\ z_4 \\ 1 \end{pmatrix} \quad (3.2)$$

Where  $\lambda, \mu$  and  $\nu$  are constants. This relation can be expressed as

$$\begin{pmatrix} x_1 & x_2 & x_3 \\ z_1 & z_2 & z_3 \\ 1 & 1 & 1 \end{pmatrix} \begin{pmatrix} \lambda \\ \mu \\ \nu \end{pmatrix} = \begin{pmatrix} x_4 \\ z_4 \\ 1 \end{pmatrix} \quad (3.3)$$

After solving for  $\lambda, \mu$  and  $\nu$  the matrix  $A$  can be constructed

$$\mathbf{A} = \begin{pmatrix} \lambda x_1 & \mu x_2 & \nu x_3 \\ \lambda z_1 & \mu z_2 & \nu z_3 \\ \lambda & \mu & \nu \end{pmatrix} \quad (3.4)$$

The matrix  $\mathbf{A}$  maps basis vectors to specific points, so that:

$$\begin{aligned}\mathbf{A}(100) &\mapsto k_1(x_1, z_1, 1) \\ \mathbf{A}(010) &\mapsto k_2(x_2, z_2, 1) \\ \mathbf{A}(001) &\mapsto k_3(x_3, z_3, 1) \\ \mathbf{A}(111) &\mapsto (x_4, z_4, 1)\end{aligned}$$

Since  $\mathbf{A}$  maps basis vectors to augmented positions,  $\mathbf{A}^{-1}$  decomposes an augmented position into basis vectors. Now, the calibration experiment provides control signals  $(V_{x_i}, V_{z_i})$  which can be transformed to augmented vectors  $\mathbf{a}$  and treated in the same way. Specifically,  $a(V_{x_1}, V_{z_1}, 1) + b(V_{x_2}, V_{z_2}, 1) + c(V_{x_3}, V_{z_3}, 1) = (V_{x_4}, V_{z_4}, 1)$  for constants  $a, b$  and  $c$  so

$$\begin{pmatrix} a \\ b \\ c \end{pmatrix} = \begin{pmatrix} V_{x_1} & V_{x_2} & V_{x_3} \\ V_{z_1} & V_{z_2} & V_{z_3} \\ 1 & 1 & 1 \end{pmatrix}^{-1} \begin{pmatrix} V_{x_4} \\ V_{z_4} \\ 1 \end{pmatrix} \quad (3.5)$$

The matrix  $\mathbf{B}$  can be created, in the same way that  $\mathbf{A}$  was

$$\mathbf{B} = \begin{pmatrix} ax_1 & bx_2 & cx_3 \\ az_1 & bz_2 & cz_3 \\ a & b & c \end{pmatrix} \quad (3.6)$$

$\mathbf{B}$  maps from basis vectors to augmented signals, so that  $\mathbf{B}(111) = (V_{x_4}, V_{z_4})$ . To compute the projective transform of an illumination position  $\mathbf{r} = (x, z)$  to the required control signal  $\mathbf{V} = (V_x, V_z)$ , we simply need to convert the augmented position to basis vectors using  $\mathbf{A}^{-1}\tilde{\mathbf{r}}$ , and the basis vectors to control signals using  $\mathbf{B}$  with dehomogenisation. It is useful to use the homography matrix  $\mathbf{H} = \mathbf{BA}^{-1}$ , so that  $\tilde{\mathbf{V}} = \mathbf{H}\tilde{\mathbf{r}}$ , or

$$\begin{pmatrix} \widetilde{V}_x \\ \widetilde{V}_z \\ k \end{pmatrix} = \begin{pmatrix} aV_{x_1} & bV_{x_2} & cV_{x_3} \\ aV_{z_1} & bV_{z_2} & cV_{z_3} \\ a & b & c \end{pmatrix} \begin{pmatrix} 0 & 1 & 0 \\ -z_1 & z_2 & z_3 \\ -1 & 1 & 1 \end{pmatrix}^{-1} \begin{pmatrix} x \\ z \\ 1 \end{pmatrix} \quad (3.7)$$

where the  $x$  range is normalised to run from  $x_1 = x_3 = 0$  to  $x_2 = x_4 = 1$ , and  $\mathbf{A}^{-1}$  is heavily simplified by solving for  $\lambda$ ,  $\mu$  and  $\nu$ . Finally

$$\begin{pmatrix} V_x \\ V_z \end{pmatrix} = \frac{1}{k} \begin{pmatrix} \widetilde{V}_x \\ \widetilde{V}_z \end{pmatrix} \quad (3.8)$$

rescales homogenous voltages to real output voltages. Non-extrema points can therefore be interpolated to create signal trains rather than point-wise; for higher-order corrections point-wise generation would be necessary.

## 3.1 Experimental Implementation and Verification

### 3.1.1 iSPIM Design

All demonstrations of the 4 pt correction were performed on an iSPIM (*inverted Selective Plane Imaging Microscope*). A (*Coherent Obis 561nm*) laser was used as the beam source. A pair of galvanometric mirrors (*Cambridge Technology*) were used to produce 2D beam steering via an image relay, this approach is well established in scanning microscopy and is known to introduce ordinarily negligible field curvature. A telecentric scan lens (*A1 Scan Lens* from Nikon) was used to convert beam angle to beam position; within the observation volume this acts to keep the sweeping beam parallel for a homogenous illumination and background. A (*10x 0.3 NA Nikon*) water dipping objective was used for excitation and mounted at right angles to a (*25x 1.1 NA*) Nikon LWD water immersion objective. The fluorescence collected by the detection objective is then imaged onto a Hamamatsu sCMOS Orca Flash 4. A piezo scanner (*Physik Instrumente P-726 PIFOC high-load objective scanner*) was used to manually move the detection objective to match the detection focal plane to the excitation plane.

### 3.1.2 Scan lens characterisation

To accurately measure the deviation solely caused by the scanning system, a camera (Thorlabs DCC1545M) was mounted directly after the scan lens and an attenuated beam was imaged directly onto the sensor. The full range of the scanning unit was considered by incrementing mirror control voltages ( $V_x, V_z$ ) linearly in input space. and imaging the illumination beam in  $xz$  for each step, as shown in Figure 3.2a. Each beam profile was fit with a 2D Gaussian to create a map of  $xz$  illumination positions corresponding to constant steps in scan lens. Figure 3.2b and 3.2c show the residual deviation from desired positions when using a 4 pt and 3 pt registration respectively. The 4 pt correction is more faithful to experimental values. The figure verifies that a 4 pt correction produce a more valid fitting for a beam scanned across a telecentric lens, with a more significant improvement becoming apparent when using a larger region of the scan lens.

### 3.1.3 *in situ* characterisation

In real samples for light-sheet microscopy, a mismatch between the detection plane and the illumination plane can reduce image fidelity due to decreased illumination in the imaging plane as well as excess background fluorescence. Figures 3.3 show the 4 pt registration largely eliminates this mismatch for real samples including fluorescent beads, dyes and a model organism.

In Figure 3.3 a-b Fluorescent beads (TetraSpeck 100nm Microspheres) were dispersed in 1.5% agarose at 1:1000 concentration and imaged using a 3 pt and a 4 pt registration. Each bead (of  $\sim 500$ ) was localised in 3D and its peak fluorescence intensity was compared in the 4 pt and 3 pt case, and was found to be, on average, 42% higher across the entire volume ( $512 \mu\text{m} \times 512 \mu\text{m} \times 100 \mu\text{m}$ ) for the 4 pt registration. For a  $10 \mu\text{m}$  light-sheet this corresponds to an axial light-sheet mismatch of  $6.9 \mu\text{m}$  on average, for the 3 pt case. The experiment from Figure 3.2 was repeated in the light-sheet microscope using dye solution for Figure 3.3c. The scanning beam was paused and iterated again through discrete positions in the imaging volume. Each record fluorescent dye image was characterised by a focus measure, obtained by finding the intensity maximum through the focus of the light-sheet for each beam position. As expected, greater depth degraded how well matched the beam was to the focal plane more sharply for the 3 pt correction than the 4 pt.

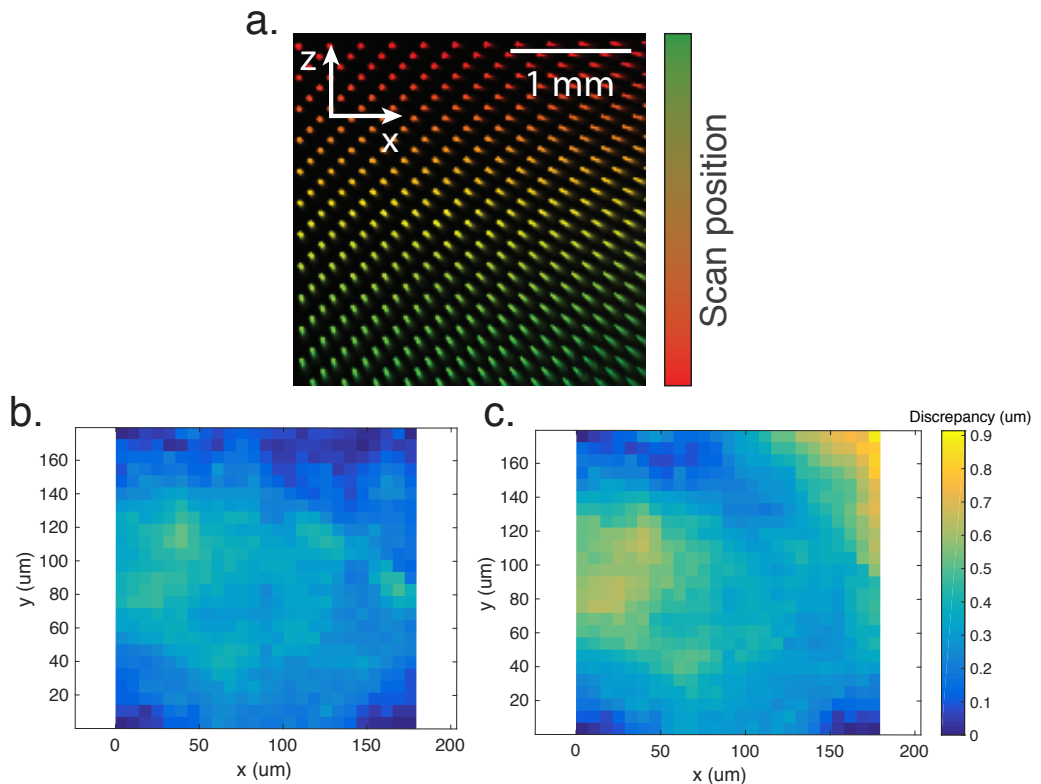


**Fig. 3.2 Scan lens characterisation** | Figure (a) shows the Illumination profile in the  $xz$  plane for 400 scan positions, with a 3 pt registration. The beam positions in (a) were each localised by fitting a 2D Gaussian. The identified positions using a 3 pt (c) and 4 pt (b) show that the positional discrepancy of the 3 pt method is largely fixed by the 4 pt registration.

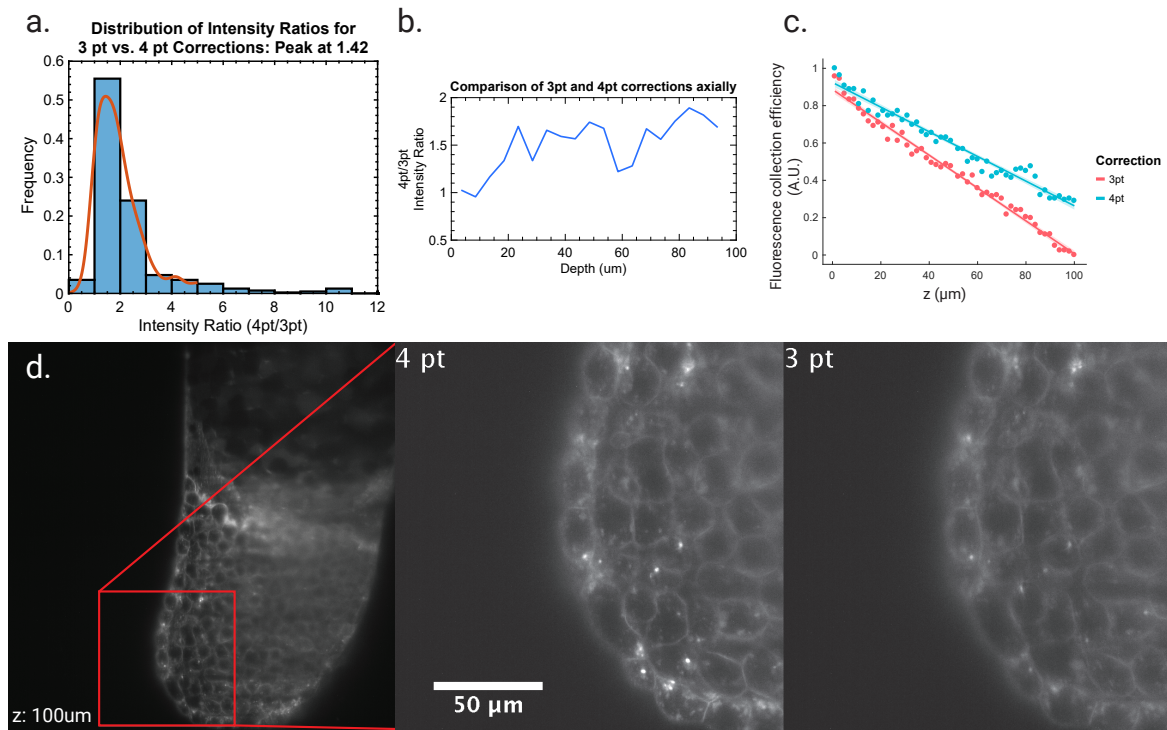


Fig. 3.3 *in situ* characterisation | (a-b) Ratios of intensity maxima of localised fluorescent bead images were compared in 3D observation volumes using 3 and 4 pt corrections. (a) These ratios show an average 42% increase in contrast for the 4 pt. case, with an increasing effect when traveling axially (b). (c) The corresponding graph for a beam scanned through dye solution also demonstrates greater light capture efficiency which becomes more significant with depth. The image maxima was taken as a good measure of beam to image plane focus. In (d) we show a transgenic Zebrafish expressing mCherry:beta-actinCAAX, in which the membrane contrast is substantially improved by the 4 pt registration.

The advantages of using a 4 pt correction were then finally demonstrated in Zebrafish (*Danio rerio*), a model organism ubiquitous in light-sheet imaging. The sample used in Figure 3.3d was transgenically expressing mCherry near the cellular membrane (Beta-actin: mcherryCAAX) and mounted in 1.2 % agarose; the sample itself was 4 hours post-fertilisation.

## 3.2 Conclusions

Considerations in registration between detection and illumination volumes[29] are becoming increasingly pertinent with the current trends of exceptionally large samples[30] being imaged at diffraction limited resolution and at depth[31, 32].

Advances in cameras[33, 34], optics[35] and fast piezo technology will further exaggerate errors introduced when using linearly generated waveforms in the next generation of light-sheet microscope.

We have demonstrated that, for iSPIM systems using virtual light-sheets, a 4 pt correction (non-linear waveform generation) versus a 3 pt correction (affine waveform generation) will better counteract errors introduced by beam scanning optics, conveniently and for minimal computational cost.



## **Chapter 4**

# **Light-sheet microscopy combined with remote force measurements**

How multicellular organisms enact the morphogenetic programmes that ensure their characteristic forms remains an enigma. Genetic screens have yielded an array of essential structural, patterning and signalling pathways with which morphogenesis is orchestrated. However, morphogenesis is ultimately a physical phenomenon that requires a physical explanation. In vivo imaging of morphogenesis allows measurements that reveal stereotypical patterns in the cellular behaviour by individual and groups of cells. These are indicative of active force generation but are insufficient to construct a quantitative explanation of where forces are generated and how forces propagate within and between tissues. To overcome these limitations, we require a quantitative characterisation of the physical properties of the tissues involved. Only with this knowledge are we able to understand how forces propagate within tissues to bring about morphogenesis. Measurements of the properties of individual cells () and for bulk tissues () have revealed both viscoelastic or visco-elasto-plastic solids (). [Cell autonomous force generation uses actomyosin-based contractile activity. – need to mention intrinsic forces someplace] Bulk tissue properties can be estimated using atomic force microscopy to investigate a tissue surface. Alternatively, micropipette aspiration can probe dissociated cells or explants, however deep tissue cannot be assessed directly. More recently, techniques have been developed to measure tissue stress and viscoelastic properties, utilising laser ablation, oil droplets, or embedding tissue explants in matrix gel. Most recently, ferrofluid droplets have shown that local tissue properties, that change regarding the tissue localisation. We are still in need of methods that can give a repeated real-time readout of physical properties and relate

those measurements to the underlying morphogenetic behaviour. [\*\*What do we say that makes us different to oil droplets?]

We sought a method that can give a non-destructive, quantitative measurement of local tissue physical properties at the length scale of a few cells, completed with seconds to minutes and repeatable over developmentally-significant periods. We chose to use biologically-compatible paramagnetic beads, implanted into the developing zebrafish embryo. A four-pole electromagnetic device was built that produces a controlled magnetic field gradient in 3D, such that a bead can be moved with known force. Tracking bead movement gives the dynamic material properties of the surrounding tissue. In a first test of this approach, we have followed the emergence of the first cohesive tissue of the zebrafish blastula, between the “high” to “sphere” stages of development(). After the mid-blastula transition, mesenchymal blastomeres become first motile and adherent to form the tissue that will go on to contribute to the first morphogenetic movement of the embryo. We could show for the first time that a three-fold elevation of tissue elasticity and viscosity are associated with this development. This elevation is dependent upon E-cadherin-based adhesions and Rac-1 dependent cell protrusive activity, abrogating either interfered with these developmental changes. Interestingly, reducing Rho-kinase dependent cell contractility increased both tissue viscosity and elasticity and raised the number of cell protrusions. To better comprehend the cellular basis for the physical properties detected by our new method, we combined magnetic tweezers with light sheet microscopy. Together, this permitted us to correlate a viscoelasticity with cell shape change and a viscosity with cell rearrangements, both cellular changes reduce as tissue elasticity and viscosity increase. We can now assign the viscoelastic component predominantly to cell shape change and viscosity to cell rearrangement. [Some of this really belongs in the discussion but will leave here for now] [If stiffness is explained by cell volume, then effect should be proportional to change in  $r$ ,  $r$  decreases just a few \*\*\* how much “plastic” change is rearrangement of extracellular space? \*\*\*

## **4.1 Tissue dynamics in developing organisms**

### **4.1.1 Embryonic rheology**

### **4.2 Methods of measuring tissue dynamics**

### **4.3 Magnetic tweezers combined with Light-sheet microscopy**

#### **4.3.1 Design**

### **4.4 Results**

### **4.5 Discussion**



# References

- [1] H Siedentpf and R Zsigmondy. Über sichtbarmachung und groessenbestimmung ultramikroskopischer teilchen, mit besonderer anwendung auf goldrubiinglaesern. 10:1–39.
- [2] A. H. Voie, D. H. Burns, and F. A. Spelman. Orthogonal-plane fluorescence optical sectioning: Three-dimensional imaging of macroscopic biological specimens. 170(3):229–236. bibtex: voie\_orthogonal-plane\_1993.
- [3] Jan Huisken, Jim Swoger, Filippo Del Bene, Joachim Wittbrodt, and Ernst H. K. Stelzer. Optical sectioning deep inside live embryos by selective plane illumination microscopy. 305(5686):1007–1009.
- [4] Philipp J Keller, Annette D Schmidt, Anthony Santella, Khaled Khairy, Zhirong Bao, Joachim Wittbrodt, and Ernst H K Stelzer. Fast, high-contrast imaging of animal development with scanned light sheet-based structured-illumination microscopy. 7(8):637–42.
- [5] Peter J Verveer, Jim Swoger, Francesco Pampaloni, Klaus Greger, Marco Marcelllo, and Ernst H K Stelzer. High-resolution three-dimensional imaging of large specimens with light sheet-based microscopy. 4(4):311–313.
- [6] Michaela Mickoleit, Benjamin Schmid, Michael Weber, Florian O Fahrbach, Sonja Hombach, Sven Reischauer, and Jan Huisken. High-resolution reconstruction of the beating zebrafish heart. 11(9):1–6.
- [7] Jaroslav Icha, Christopher Schmied, Jaydeep Sidhaye, Pavel Tomancak, Stephan Preibisch, and Caren Norden. Using light sheet fluorescence microscopy to image zebrafish eye development. (110).
- [8] Philipp J. Keller and Misha B. Ahrens. Visualizing whole-brain activity and development at the single-cell level using light-sheet microscopy. 85(3):462–483.
- [9] Takehiko Ichikawa, Kenichi Nakazato, Philipp J Keller, Hiroko Kajiura-Kobayashi, Ernst H K Stelzer, Atsushi Mochizuki, and Shigenori Nonaka. Live imaging and quantitative analysis of gastrulation in mouse embryos using light-sheet microscopy and 3d tracking tools. 9(3):575–85.
- [10] Daniel Von Wangenheim, Jens Fangerau, Alexander Schmitz, Richard S Smith, Heike Leitte, Ernst H K Stelzer, and Alexis Maizel. Rules and self-organizing properties of post-embryonic plant organ cell division patterns. pages 1–11.

- [11] Jérémie Capoulade, Malte Wachsmuth, Lars Hufnagel, and Michael Knop. Quantitative fluorescence imaging of protein diffusion and interaction in living cells. 29(9):835–839.
- [12] Francesca Cella Zanacchi, Zeno Lavagnino, Michela Perrone Donnorso, Alessio Del Bue, Laura Furia, Mario Faretta, and Alberto Diaspro. Live-cell 3d super-resolution imaging in thick biological samples. 8(12):1047–1049.
- [13] Philipp J Keller and Ernst HK Stelzer. Quantitative *in vivo* imaging of entire embryos with digital scanned laser light sheet fluorescence microscopy. 18(6):624–632.
- [14] B.-C. Chen, Wesley R. Legant, K. Wang, Lin Shao, Daniel E. Milkie, Michael W. Davidson, Chris Janetopoulos, Xufeng S. Wu, J. A. Hammer, Zhe Liu, Brian P. English, Y. Mimori-Kiyosue, Daniel P. Romero, Alex T. Ritter, J. Lippincott-Schwartz, L. Fritz-Laylin, R. Dyche Mullins, Diana M. Mitchell, A.-C. Reymann, Joshua N. Bembeneck, R. Bohme, Stephan W. Grill, Jennifer T. Wang, Geraldine Seydoux, U. Serdar Tulu, Daniel P. Kiehart, Eric Betzig, A.-C. Reymann, R. Bohme, Stephan W. Grill, Jennifer T. Wang, Geraldine Seydoux, U. Serdar Tulu, Daniel P. Kiehart, and Eric Betzig. Lattice light-sheet microscopy: Imaging molecules to embryos at high spatiotemporal resolution. 346(6208):1257998–1257998.
- [15] Florian O Fahrbach, Fabian F Voigt, Benjamin Schmid, Fritjof Helmchen, and Jan Huisken. Rapid 3d light-sheet microscopy with a tunable lens. 21(18):21010–21026.
- [16] Jim Swoger, Peter Verveer, Klaus Greger, Jan Huisken, and Ernst H. K. Stelzer. Multi-view image fusion improves resolution in three-dimensional microscopy. 15(13):8029–8029.
- [17] Abhishek Kumar, Yicong Wu, Ryan Christensen, Panagiotis Chandris, William Gandler, Evan McCready, Alexandra Bokinsky, Daniel a Colón-Ramos, Zhirong Bao, Matthew McAuliffe, Gary Rondeau, and Hari Shroff. Dual-view plane illumination microscopy for rapid and spatially isotropic imaging. 9(11):2555–73. bibtex: kumar\_dual-view\_2014.
- [18] Tongcang Li, Sadao Ota, Jeongmin Kim, Zi Jing Wong, Yuan Wang, Xiaobo Yin, and Xiang Zhang. Axial plane optical microscopy. 4:7253–7253.
- [19] C. Dunsby. Optically sectioned imaging by oblique plane microscopy. 16(25):20306. bibtex: dunsby\_optically\_2008.
- [20] Martin Plöschner, Věra Kollárová, Zbyněk Dostál, Jonathan Nylk, Thomas Barton-Owen, David E. K. Ferrier, Radim Chmelík, Kishan Dholakia, and Tomáš Čižmár. Multimode fibre: Light-sheet microscopy at the tip of a needle. 5:18050–18050.
- [21] Remi Galland, Gianluca Grenci, Ajay Aravind, Virgile Viasnoff, Vincent Studer, and Jean-Baptiste Sibarita. 3d high- and super-resolution imaging using single-objective SPIM. 12:1–13. bibtex: galland\_3d\_2015.

- [22] Qinyi Fu, Benjamin L. Martin, David Q. Matus, and Liang Gao. Imaging multicellular specimens with real-time optimized tiling light-sheet selective plane illumination microscopy. 7:11088–11088. bibtex: fu\_imaging\_2016.
- [23] Liang Gao, Lin Shao, Bi-Chang Chen, and Eric Betzig. 3d live fluorescence imaging of cellular dynamics using bessel beam plane illumination microscopy. 9(5):1083–101.
- [24] Tom Vettenburg, Heather I C Dalgarno, Jonathan Nylk, Clara Coll-Lladó, David E K Ferrier, Tomáš Cižmár, Frank J Gunn-Moore, and Kishan Dholakia. Light-sheet microscopy using an airy beam. 11(5):541–4.
- [25] Mike Friedrich, Qiang Gan, Vladimir Ermolayev, and Gregory S. Harms. STED-SPIM: Stimulated emission depletion improves sheet illumination microscopy resolution. 100(8):L43–L45. bibtex: friedrich\_sted-spim:\_2011.
- [26] Peter G Pitrone, Johannes Schindelin, Luke Stuyvenberg, Stephan Preibisch, Michael Weber, Kevin W Eliceiri, Jan Huisken, and Pavel Tomancak. OpenSPIM: an open-access light-sheet microscopy platform. 10(7):598–9.
- [27] Philipp J Keller, Annette D Schmidt, Anthony Santella, Khaled Khairy, Zhirong Bao, Joachim Wittbrodt, and Ernst H K Stelzer. Fast, high-contrast imaging of animal development with scanned light sheet-based structured-illumination microscopy. 7(8):637–42.
- [28] Barbara Zitová and Jan Flusser. Image registration methods: A survey. 21(11):977–1000.
- [29] Loïc A. Royer, William C. Lemon, Raghav K. Chhetri, Yinan Wan, Michael Coleman, Eugene W. Myers, and Philipp J. Keller. Adaptive light-sheet microscopy for long-term, high-resolution imaging in living organisms. advance online publication.
- [30] Fei Chen, Paul W Tillberg, and Edward S Boyden. Expansion microscopy. 347:543–548. bibtex: chen\_expansion\_2015.
- [31] Kai Wang, Wenzhi Sun, Christopher T. Richie, Brandon K. Harvey, Eric Betzig, and Na Ji. Direct wavefront sensing for high-resolution *in vivo* imaging in scattering tissue. 6:7276. bibtex: wang\_direct\_2015.
- [32] Thai V Truong, Willy Supatto, David S Koos, John M Choi, and Scott E Fraser. Deep and fast live imaging with two-photon scanned light-sheet microscopy. 8(9):757–60.
- [33] Guoan Zheng, Xiaoze Ou, and Changhuei Yang. 0.5 gigapixel microscopy using a flatbed scanner. 5(1):1–8.
- [34] D. J. Brady, M. E. Gehm, R. A. Stack, D. L. Marks, D. S. Kittle, D. R. Golish, E. M. Vera, and S. D. Feller. Multiscale gigapixel photography. 486(7403):386–389.
- [35] Nicholas James Sofroniew, Daniel Flickinger, Jonathan King, and Karel Svoboda. A large field of view two-photon mesoscope with subcellular resolution for *in vivo* imaging. 5:e14472.



# **Appendix A**

## **How to install L<sup>A</sup>T<sub>E</sub>X**

### **Windows OS**

#### **TeXLive package - full version**

1. Download the TeXLive ISO (2.2GB) from  
<https://www.tug.org/texlive/>
2. Download WinCDEmu (if you don't have a virtual drive) from  
<http://wincdemu.sysprogs.org/download/>
3. To install Windows CD Emulator follow the instructions at  
<http://wincdemu.sysprogs.org/tutorials/install/>
4. Right click the iso and mount it using the WinCDEmu as shown in  
<http://wincdemu.sysprogs.org/tutorials/mount/>
5. Open your virtual drive and run setup.pl

or

#### **Basic MiK<sub>E</sub>X - T<sub>E</sub>X distribution**

1. Download Basic-MiK<sub>E</sub>X(32bit or 64bit) from  
<http://miktex.org/download>
2. Run the installer

3. To add a new package go to Start » All Programs » MikTex » Maintenance (Admin) and choose Package Manager
4. Select or search for packages to install

## **TexStudio - $\text{\TeX}$ editor**

1. Download TexStudio from  
<http://texstudio.sourceforge.net/#downloads>
2. Run the installer

## **Mac OS X**

### **MacTeX - $\text{\TeX}$ distribution**

1. Download the file from  
<https://www.tug.org/mactex/>
2. Extract and double click to run the installer. It does the entire configuration, sit back and relax.

## **TexStudio - $\text{\TeX}$ editor**

1. Download TexStudio from  
<http://texstudio.sourceforge.net/#downloads>
2. Extract and Start

## **Unix/Linux**

### **TeXLive - $\text{\TeX}$ distribution**

#### **Getting the distribution:**

1. TeXLive can be downloaded from  
<http://www.tug.org/texlive/acquire-netinstall.html>.

2. TexLive is provided by most operating system you can use (rpm, apt-get or yum) to get TexLive distributions

## Installation

1. Mount the ISO file in the mnt directory

```
mount -t iso9660 -o ro,loop,noauto /your/texlive####.iso /mnt
```

2. Install wget on your OS (use rpm, apt-get or yum install)

3. Run the installer script install-tl.

```
cd /your/download/directory  
./install-tl
```

4. Enter command 'i' for installation

5. Post-Installation configuration:

<http://www.tug.org/texlive/doc/texlive-en/texlive-en.html#x1-320003.4.1>

6. Set the path for the directory of TexLive binaries in your .bashrc file

## For 32bit OS

For Bourne-compatible shells such as bash, and using Intel x86 GNU/Linux and a default directory setup as an example, the file to edit might be

```
edit $~/.bashrc file and add following lines  
PATH=/usr/local/texlive/2011/bin/i386-linux:$PATH;  
export PATH  
MANPATH=/usr/local/texlive/2011/texmf/doc/man:$MANPATH;  
export MANPATH  
INFOPATH=/usr/local/texlive/2011/texmf/doc/info:$INFOPATH;  
export INFOPATH
```

**For 64bit OS**

```
edit $~/.bashrc file and add following lines  
PATH=/usr/local/texlive/2011/bin/x86_64-linux:$PATH;  
export PATH  
MANPATH=/usr/local/texlive/2011/texmf/doc/man:$MANPATH;  
export MANPATH  
INFOPATH=/usr/local/texlive/2011/texmf/doc/info:$INFOPATH;  
export INFOPATH
```

**Fedora/RedHat/CentOS:**

```
sudo yum install texlive  
sudo yum install psutils
```

**SUSE:**

```
sudo zypper install texlive
```

**Debian/Ubuntu:**

```
sudo apt-get install texlive texlive-latex-extra  
sudo apt-get install psutils
```

# **Appendix B**

## **Installing the CUED class file**

$\text{\LaTeX}.\text{cls}$  files can be accessed system-wide when they are placed in the  $\langle\text{texmf}\rangle/\text{tex}/\text{latex}$  directory, where  $\langle\text{texmf}\rangle$  is the root directory of the user's  $\text{\TeX}$  installation. On systems that have a local texmf tree ( $\langle\text{texmflocal}\rangle$ ), which may be named "texmf-local" or "localtexmf", it may be advisable to install packages in  $\langle\text{texmflocal}\rangle$ , rather than  $\langle\text{texmf}\rangle$  as the contents of the former, unlike that of the latter, are preserved after the  $\text{\LaTeX}$  system is reinstalled and/or upgraded.

It is recommended that the user create a subdirectory  $\langle\text{texmf}\rangle/\text{tex}/\text{latex}/\text{CUED}$  for all CUED related  $\text{\LaTeX}$  class and package files. On some  $\text{\LaTeX}$  systems, the directory look-up tables will need to be refreshed after making additions or deletions to the system files. For  $\text{\TeX}{}^{\text{Live}}$  systems this is accomplished via executing "texhash" as root. MIK $\text{\TeX}$  users can run "initexmf -u" to accomplish the same thing.

Users not willing or able to install the files system-wide can install them in their personal directories, but will then have to provide the path (full or relative) in addition to the filename when referring to them in  $\text{\LaTeX}$ .

